eNeuro

Research Article: New Research | Neuronal Excitability

A Novel View on the Role of Intracellular Tails in Surface Delivery of the Potassium-Chloride Cotransporter KCC2

N-Terminus Determines KCC2 Cell Surface Delivery

Perrine Friedel[1], Anastasia Ludwig[2], Christophe Pellegrino[1], Morgane Agez[3], Anass Jawhari[3], Claudio Rivera[1,2] and Igor Medina[1]

[1]*INMED, Aix-Marseille Univversity, INSERM, Marseille, France*
[2]*Neuroscience Center, University of Helsinki, Helsinki, Finland*
[3]*CALIXAR, 60 Avenue Rockefeller, Lyon, 69008, France*

DOI: 10.1523/ENEURO.0055-17.2017

Received: 15 February 2017

Revised: 20 June 2017

Accepted: 4 July 2017

Published: 12 July 2017

Author contribution: Conceptualization, P.F and I.M; Methodology and experimental design, P.F, A.L, C.P, M.A, A.J, C.R and I.M.; Investigation, P.F, A.L, C.P, M.A, A.J, and I.M.; Writing, P.F, A.L, A.J and I.M.; Funding Acquisition, C.R and I.M.; Supervision, C.R and I.M.; Project Administration, I.M.

Funding: Arthritis National Research Foundation (ANRF)
100000964
TRAUMEP ANR 13-BSV4-0012-01

Funding: Academy of Finland | Biotieteiden ja Ympäristön Tutkimuksen Toimikunta (Forskningsrådet för Biovetenskap och Miljö)
501100005876
SA 259799

Funding: Institut National de la Santé et de la Recherche Médicale (Inserm)
501100001677
INSERM-CR-PACA-FEDER

Conflict of Interest: The authors declare that they have no conflicts of interest.

This work was supported by the Institut National de la Santé et de la Recherche Médicale (INSERM) I.M and C.R, Aix-Marseille University (AMU) to I.M and C.R, University of Helsinki (C.R), the Agence Nationale de la Recherche (ANR) (TRAUMEP ANR 13-BSV4-0012-01 to C.R. and I.M), Academy of Finland (SA 259799 to CR). P.F. was supported by an INSERM-CR-PACA-FEDER grant and A.L. was supported by the Academy of Finland (SA 250742).

Guidelines of the Animal Care: All manipulations with animals were performed in agreement with the guidelines of the Animal Care and Use Committee of INSERM (Institut National de la Santé et de la Recherche Médicale).

Correspondence should be addressed to Igor Medina, INMED/INSERM Unité 901, 163 Route de Luminy, 13273 Marseille, France. Phone: (33) 4 91 82 81 07; fax: (33) 4 91 82 81 01; E-mail: igor.medyna@inserm.fr

Cite as: eNeuro 2017; 10.1523/ENEURO.0055-17.2017

1. **Manuscript title:** A Novel View on the Role of Intracellular Tails in Surface Delivery of the Potassium-Chloride Cotransporter KCC2.
2. **Abbreviated title:** *N*-Terminus Determines KCC2 Cell Surface Delivery.
3. **Authors:** Perrine Friedel[1]‡, Anastasia Ludwig[2]§, Christophe Pellegrino[1], Morgane Agez[3], Anass Jawhari[3], Claudio Rivera[1,2], Igor Medina[1*]

[1]INMED, Aix-Marseille Univ, INSERM, Marseille, France
[2]Neuroscience Center, University of Helsinki, Helsinki, Finland
[3]CALIXAR, 60 avenue Rockefeller, 69008, Lyon, France
‡ = present address (Department of Cellular and Molecular Physiology, Yale School of Medicine, New Haven, Connecticut, USA)
§ = present address (Ecole Normale Supérieure, Institut de Biologie de l'ENS (IBENS), Inserm U1024, CNRS 8197, Biologie Cellulaire de la Synapse, 46 rue d'Ulm, Paris 75005, France)
4. **Author contribution:** Conceptualization, P.F and I.M; Methodology and experimental design, P.F, A.L, C.P, M.A, A.J, C.R and I.M.; Investigation, P.F, A.L, C.P, M.A, A.J, and I.M.; Writing, P.F, A.L, A.J and I.M.; Funding Acquisition, C.R and I.M.; Supervision, C.R and I.M.; Project Administration, I.M.
5. **Correspondence should be addressed to**: Dr. Igor Medina, INMED / INSERM Unité 901, 163 Route de Luminy, 13273 Marseille, France. Phone: (33) 4 91 82 81 07; fax: (33) 4 91 82 81 01; E-mail: **igor.medyna@inserm.fr**

6. **Number of Figures:** 8;
7. **Number of Tables**: 4;
8. **Number of Multimedia** 0;
9. **Number of words for Abstract** 164;
10. **Number of words for Significance Statement:** 69;
11. **Number of words for Introduction:** 454;
12. **Number of words for Discussion:** 975.

13. **Acknowledgements:** We are grateful to Galyna Medyna and Kacey Rajkovich for editing and Lucie Pisella for critical reading of the manuscript. This work was supported by the Institut National de la Santé et de la Recherche Médicale (INSERM) I.M and C.R, Aix-Marseille University (AMU) to I.M and C.R, University of Helsinki (C.R), the Agence Nationale de la Recherche (ANR) (TRAUMEP ANR 13-BSV4-0012-01 to C.R. and I.M), Academy of Finland (SA 259799 to CR). P.F. was supported by an INSERM-CR-PACA-FEDER grant and A.L. was supported by the Academy of Finland (SA 250742).
14. **Conflict of interest:** The authors declare that they have no conflicts of interest with the contents of this article.
15. **Funding sources:** This work was supported by the Institut National de la Santé et de la Recherche Médicale (INSERM) I.M and C.R, Aix-Marseille University (AMU) to I.M and C.R, University of Helsinki (C.R), the Agence Nationale de la Recherche (ANR) (TRAUMEP ANR 13-BSV4-0012-01 to C.R. and I.M), Academy of Finland (SA 259799 to CR). P.F. was supported by an INSERM-CR-PACA-FEDER grant and A.L. was supported by the Academy of Finland (SA 250742).
16. **Guidelines of the Animal Care:** All manipulations with animals were performed in agreement with the guidelines of the Animal Care and Use Committee of INSERM (Institut National de la Santé et de la Recherche Médicale).
17. **Keywords:** gamma-aminobutyric acid (GABA), chloride transport, potassium transport, cell surface protein, neuron, KCC2

A Novel View on the Role of Intracellular Tails in Surface Delivery of the Potassium-Chloride Cotransporter KCC2.

ABSTRACT

A plethora of neurological disorders are associated with alterations in the expression and localization of the potassium-chloride co-transporter type 2 (KCC2), making KCC2 a critical player in neuronal function and an attractive target for therapeutic treatment. The activity of KCC2 is determined primarily by the rates of its surface insertion and internalization. Currently the domains of KCC2 dictating its trafficking and endocytosis are unknown. Here, using live-cell immunolabelling and biotinylation of KCC2 proteins expressed either in murine neuroblastoma N2a cells, human embryonic kidney 293 cells or primary cultures of rat hippocampal neurons, we identified a novel role for the intracellular *N*- and *C*-termini in differentially regulating KCC2 surface expression. We report that the *N*-terminus is required for KCC2 insertion into the plasma membrane, while the *C*-terminus is critical for the membrane stability of KCC2. Our results provide novel insights into the structure-function role of specific KCC2 domains and open perspectives in exploring structural organization of this protein.

SIGNIFICANCE STATEMENT

The neuronal potassium-chloride co-transporter KCC2 is critically involved in numerous neurological disorders. However, the structural components that regulate KCC2 activity remain to be elucidated. Here, we describe novel and differential roles for the intracellular amino- and carboxy-terminal domains of KCC2 that dictate its plasmalemmal insertion and surface stabilization. Our findings challenge the current view on the structure-function role of the cytoplasmic regions of KCC2 and propose new targets in the search for therapeutic treatments.

INTRODUCTION

A low intracellular chloride concentration ($[Cl^-]_i$) is required for inhibitory synaptic transmission in mature neurons and is maintained by the neuron-specific potassium-chloride co-transporter type 2 (KCC2) by facilitating the export of chloride ions (Rivera et al., 1999). Decreased KCC2 activity is linked to the etiology of several neurological disorders including epilepsy, acute trauma, ischemia, post-surgery complications and neuropathic pain (Blaesse et al., 2009; Kahle et al., 2013; Medina et al., 2014). In both physiological and pathological conditions, the major mechanism controlling KCC2 function relies on the

control of its surface expression (Chamma et al., 2012; Kahle et al., 2013; Medina et al., 2014). While recent studies have identified a number of KCC2 amino acid residues involved in its internalization, the domain(s) of KCC2 that regulate its insertion into the plasma membrane remain unknown (Lee et al., 2007, 2010; Kahle et al., 2014; Puskarjov et al., 2014; Weber et al., 2014; Friedel et al., 2015; Stödberg et al., 2015).

The mammalian *KCC2* gene (alias *Slc12a5*) generates two major isoforms, KCC2a and KCC2b, which differ in their amino (*N*)-termini (Uvarov et al., 2007) and their developmental and spatial profile of expression (Markkanen et al., 2014). Historically, the first KCC2 molecule discovered by Payne et al., in 1996 was actually the isoform KCC2b; it is nowadays considered as the major and most important isoform in the adult brain and spinal cord (Payne et al., 1996; Rivera et al., 1999; Stein et al., 2004; Markkanen et al., 2014). The mice with knocked-out KCC2b are characterized by an increased epileptiform-like neuronal network activity and die at juvenile age of 2-3 postnatal weeks (Woo et al., 2002). The KCC2a isoform is expressed in immature neurons of all brain regions, but is absent or little expressed in mature cortex, hippocampus, thalamus, and cerebellar cortex (Uvarov et al., 2007; Markkanen et al., 2014). The mice with knocked-out KCC2a appear grossly normal although their phenotype was not characterized in details (Markkanen et al., 2014). Interestingly, a recent study reported the identification of 11 additional alternative transcripts of KCC2 that are potentially associated with psychiatric disorders in human; however, their expression profile and functional importance have not been entirely studied yet (Tao et al., 2012). Hydrophobicity analysis of KCC2b amino acid sequence predicted a 2D structure composed of 12 transmembrane domains flanked by intracellular/cytoplasmic *N*- and carboxy (*C*-) termini (Payne et al., 1996). The putative transmembrane region of KCC2 is composed of 532 amino acids and *N*- and *C*-termini count respectively 102 and 482 amino acids (Payne et al., 1996).

Here, we identified the region on KCC2b isoform that contributes to the surface insertion of the molecule. Using live-cell immunolabelling, we analyzed the surface expression of KCC2b proteins harboring an extracellular pHluorin tag (KCC2-pH_{ext}) and missing either intracellular *N*- or *C*- terminus. We found that the deletion of the *N*-terminal part of KCC2-pH_{ext} (ΔNTD-KCC2-pH_{ext}) altered the delivery of the transporter into the plasma membrane of cultured hippocampal neurons, neuron-derived cell line (N2a) and human embryonic kidney 293 cells (HEK293) cells. Conversely, the construct composed of the *N*-terminus portion and 12 transmembrane domains only - *i.e.* deletion of the entire intracellular *C*-tail (ΔCTD-KCC2-pH_{ext}) - was effectively inserted into the plasma membrane. The compromised surface expression of ΔNTD-KCC2-pH_{ext} was not an artefact of the extracellular tag, as biotinylation of N2a cells overexpressing non-tagged constructs confirmed the effective surface labeling of wild-type KCC2, ΔCTD-KCC2, but not ΔNTD-KCC2 mutant. Our results identify the KCC2 *N*-terminus as a region indispensable

for plasma membrane insertion of the transporter and suggest that the large *C*-terminus tail is not critical for this process, but rather plays a role in KCC2 stabilization at the cell surface.

MATERIALS AND METHODS

All manipulations with animals were performed in agreement with the guidelines of the Animal Care and Use Committee of INSERM (Institut National de la Santé et de la Recherche Médicale).

Expression constructs – The KCC2-IRES-GFP (Chudotvorova et al., 2005), eGFP-KCC2 (Pellegrino et al., 2011) and KCC2-pH_{ext} (Kahle et al., 2014) were kindly provided by Dr Medina. The ΔNTD-KCC2 (Li et al., 2007) was obtained from Dr. Rivera. The non-tagged wild-type KCC2 (WT-KCC2) was obtained by removal of the sequence encoding the eGFP tag from eGFP-KCC2. The ΔNTD-KCC2-pH_{ext} mutant (deletion of 1-100 amino acids) was created using PCR. The ΔCTD-KCC2 mutant (deletion of KCC2's 654-1114 amino acids) was made by deleting the corresponding piece of KCC2 using BamHI endonuclease. mCherry construct was created by insertion of an ubiquitin promoter instead of CMV promoter in pmCherry vector (Clontech Laboratories, Inc.). All constructs were verified by DNA sequencing. More details on vectors and all constructs are available upon request.

Primary cultures and transfection of rat hippocampal neurons – Hippocampal neurons from 18 day Wistar rat embryos of either gender were dissociated using trypsin and plated onto poly-ethylene-imine-coated coverslips at a density of 70,000 cells cm^{-2} in minimal essential medium (MEM) supplemented with 10% NU serum (BD Biosciences, Le Pont de Claix, France), 0.45% glucose, 1 mM sodium pyruvate, 2 mM glutamine, and 10 IU ml^{-1} penicillin–streptomycin. On day 9 of culture incubation, half of the medium was changed to MEM with 2% B27 supplement (Life Technologies). Transfection of cultured neurons was performed as described by Buerli et al., (2007) and briefly summarized below. 300 µl of Opti-MEM media was mixed with 7 µl of Lipofectamine reagent 2000 (Life Technologies), 1 µl of Magnetofection CombiMag (OZ Biosciences, France) and 1.5 µg of pre-mixed DNAs encoding constructs of interest. The mixture was incubated 20 min at room temperature (RT) and thereafter distributed dropwise above the neuronal culture. Culture dishes were placed on a magnetic plate (OZ Biosciences) and incubated 40 min at 37°C, 5% CO_2. Transfection was terminated by the substitution of 70% of the incubation solution with fresh culture media. Cells were used in the experiments 3 days after transfection.

Culture and transfection of N2a and HEK293 cells – Mouse neuroblastoma cells (N2a) (ATCC, #CCL-131) and human embryonic kidney 293 cells (HEK293) (ATCC, #CRL-1573) were cultured in Dulbecco's modified Eagle's medium supplemented with 10% fetal bovine serum, 10 IU ml^{-1} penicillin–streptomycin. The cells were transfected with appropriate pcDNAs using Lipofectamine reagent 2000 (Life Technologies) according to the manufacturer's protocol and used 48-72 hours (h) after transfection.

Antibodies for immunocytochemistry – Primary antibodies used for immunocytochemistry were rabbit polyclonal anti-GFP (dilution 1:500; Molecular Probes, Life Technologies), mouse monoclonal anti-GFP (dilution 1:600; Novus Biologicals), rabbit polyclonal anti-DsRed (dilution 1:500; Takara Bio). Secondary antibodies were Cy3-conjugated goat anti-rabbit IgG (dilution 1:500; Jackson ImmunoResearch Laboratories, Inc., West Grove, PA, USA), Alexa Fluor 488-conjugated goat anti-mouse IgG (dilution 1:500; FluoProbes), Alexa Fluor 647-conjugated goat anti-rabbit IgG (dilution 1:500; Chemicon). Cell nuclei were revealed using 5-min staining with Hoechst 33258 (1µg/ml, Sigma-Aldrich).

Gramicidin perforated patch clamp recording – For estimation of $[Cl^-]_i$ in N2a cells, the cells were transfected with a mixture of two mammalian expression constructs encoding the human α1 subunit of the glycine receptor (GlyR), and KCC2-pH_{ext}, eGFP (mock) or KCC2-IRES-GFP (KCC2). For $[Cl^-]_i$ measurements in cultured neurons, 6 days *in vitro* (d.i.v.) neurons were transfected with KCC2-pH_{ext}, eGFP (mock) or KCC2-IRES-GFP (KCC2). Measurements were performed 2 or 3 days after transfection (corresponding to 8 or 9 d.i.v. neurons). Coverslips with N2a cells or neurons were placed onto the inverted microscope and perfused with an external solution (in mM): 140 NaCl, 2.5 KCl, 20 HEPES, 20 D-glucose, 2.0 CaCl2, 2.0 MgCl2, 0.02 Bumetanide, pH 7.4. For recording from neurons external solution contained 0.3 µM strychnine and 1 µM tetrodotoxin. The recording micropipettes (5 MΩ) were filled with a solution containing (in mM): 150 KCl, 10 HEPES, 20 µg/ml gramicidin A, pH 7.2. Glycine (50 µM, for recordings of N2a cells) or isoguvacine (30 µM, a selective agonist of $GABA_AR$ for recordings of neurons) was dissolved in external solution and focally applied to recorded cells through a micropipette connected to a Picospritzer (General Valve Corporation, pressure 5 p.s.i.). Recordings were done with an Axopatch-200A amplifier and pCLAMP acquisition software (Axon Instruments) in voltage-clamp mode. Data were low-pass filtered at 2 kHz and acquired at 10 kHz.

Surface immunolabeling and analysis –Prior to labeling, half of culture media was removed from dishes containing cultured neurons or cell lines and transferred to a single centrifuge tube containing polyclonal rabbit anti-GFP antibody. The obtained mixture was centrifuged 5 min at 8000 rpm, the supernatant was placed into the cell culture incubator for at least 30 min (to equilibrate with CO_2 and temperature) and distributed afterward to dishes containing neurons. Neurons exposed to the media containing primary antibody were kept in the incubator at 37°C during 2h. The incubation time was determined experimentally to obtain approximately equal amount of fluorescence intensity emitted by surface located and internalized clusters in neurons expressing WT-KCC2-pH_{ext} and revealed as described below. After labeling, cultures were transferred at RT to HEPES-buffered saline and were placed for 10 min into the thermo-isolated box at 13°C. The cells were then incubated at 13°C for 20 min with anti-rabbit Cy3-conjugated antibody that revealed the plasma membrane KCC2-pH_{ext} pool (F_m). The temperature, time, antibody concentration and secondary antibody (Cy™3 AffiniPure Goat Anti-Rabbit

IgG (H+L)) were selected to obtain reproducible staining of KCC2-pH_{ext} located on the cell surface (as shown in single plane images of Figure 3*B*, upper raw). Lowering the temperature below 10°C or increasing the incubation time with Cy3-conjugated antibody to more than 40 min resulted in damage of the plasma membrane (positive staining of neurons with eGFP-KCC2). Increasing the antibody concentration (dilution 1:200) resulted in an increase of the background fluorescence on non-transfected neurons without improving the brightness and number of clusters on the transfected ones. The staining with other secondary antibodies conjugated with Cy5, Alexa 546, Alexa 633 or Alexa 647 fluorophores was less effective. After rinsing in a HEPES-buffered saline solution for 10 min at 13°C, the cells were fixed in Antigenfix (Diapath, Martingo, Italy) for 20 min (RT), permeabilized (0.3% Triton X-100), blocked (5% goat serum) for 30 min and labeled with a second secondary antibody (anti-rabbit Alexa 647) during 1h. This staining allowed visualization of labeled internalized proteins (fluorescence signal located inside of the neuron at individual confocal Z scans, Figure 3*B*). The staining with Alexa 647 antibody revealed also labeled WT-KCC2-pH_{ext} clusters located on the cell surface (*i.e.,* Cy3-positive). This indicated that the epitopes on primary antibodies were not saturated during live-cell staining with Cy3-conjugated antibody or were unmasked during fixation/permeabilization procedure. Therefore, to dissect the "pure" internalized pool of labeled molecules, the single plane images of Alexa 647 and Cy3 emitted fluorescence were treated arithmetically afterwards as described below. To detect the total level of ectopic KCC2-related proteins expressed, the cells were finally labeled with mouse anti-GFP antibody (1h, RT) and revealed with anti-mouse Alexa 488 antibody (1h, RT).

To reveal all the clusters labeled on the cell surface (F_{all}), we omitted the live-cell staining step with the anti-rabbit Cy3-conjugated antibody and revealed labeled proteins by applying a single secondary anti-rabbit Alexa 647 antibody to fixed and permeabilized cells.

For quantitative analysis, images of labeled cells were acquired with an Olympus Fluorview-500 confocal microscope using oil-immersion objective 60x (NA1.4), zoom 3, and 15 pixels/µm image resolution). We randomly selected and focused on a transfected cell by only visualizing Alexa 488 fluorescence and then acquired Z-stack images of Alexa 488, Cy3 and Alexa 647 fluorochromes emitted fluorescence using, respectively green (excitation 488 nm, emission 505-525 nm), red (excitation 543 nm emission 560-600 nm) and infra-red (excitation 633, emission >660 nm) channels of the microscope. Each Z-stack included 10 planes of 1 µm optical thickness and taken at 0.7 µm distance between planes. The cluster properties and fluorescence intensities of each cell were analyzed with Metamorph software. First, we made subtraction between Alexa 647 and Cy3 images to isolate in each focal plane the Alexa 647 signal that was not overlapping with Cy3 fluorescence. This gave rise to additional "internalized pool" images. Second, the arithmetic summation for each Z-stack and channel was performed to collect the whole fluorescence of the different signals (Alexa 488; Cy3; internalized pool; Alexa 647). Third, a binary

mask was created for each cell from Alexa 488 image to isolate the signal coming from the transfected neuron, and the fluorescence parameters (total fluorescence, single cluster fluorescence as well as density and brightness of clusters) were analyzed for each channel (Alexa 488, Cy3, internalized pool and Alexa 647) in regions overlapping with the binary mask. The analysis parameters were the same for each experiment and all experiments were done blind.

Quantification of KCC2 mutants expression in neuronal compartments– 13 d.i.v. cultured hippocampal neurons co-transfected with mCherry and KCC2-pH$_{ext,}$ ΔNTD-KCC2-pH$_{ext}$ or ΔCTD-KCC2-pH$_{ext}$ were fixed with Antigenfix 48 hours after transfection, then permeabilized and immunolabeled using rabbit anti-DsRed polyclonal antibody and mouse anti-GFP antibody followed by Cy3-conjugated anti-rabbit and Alexa 488-conjugated anti-mouse. The confocal images of neurons were taken as described in previous paragraph and analysed using the following method. For each channel, Z-stacks of 10 planes were converted into a single image using arithmetic summation with Metamorph software and a binary mask was generated based on Cy3-emitted signal. Alexa-488 fluorescence was measured within the binary mask, normalized to Cy3 intensity and reported as the total expression of KCC2 protein. Regions of interest (ROI) were then drawn on the binary mask to identify proximal (40-60 µm from soma) and distal dendrites (150-200 µm from soma). The Alexa-488 fluorescence was measured in each ROI and normalized to the reference ROI ("ref").

SDS-PAGE and Western Blot analysis – N2a cells were plated on 35 mm cell culture dishes 24 h before transfection to obtain 80% of confluence at the day of transfection. Transfections with 1.5 µg per dish of DNA encoding KCC2, KCC2-pH$_{ext}$, ΔNTD-KCC2, ΔNTD-KCC2-pH$_{ext}$, ΔCTD-KCC2, ΔCTD-KCC2-pH$_{ext}$ or pcDNA3.1 (mock) were performed using Lipofectamine 2000 according to manufacturer's protocol. 36 h after transfection, the cells were gently rinsed with ice-cold phosphate-buffered saline (PBS) complemented with iodoacetamide 10 mM, and Complete Protease Inhibitor Cocktail (Roche), scraped and centrifuged 10 min at 3000 g (4°C). The pellet was dissolved in ice-cold RIPA buffer (NaCl 150 mM; TritonX-100 1%; DOC 0.5%; SDS 0.1%; Tris-HCl 50 mM; iodoacetamide 10 mM, pH 8.0) complemented with Complete Protease Inhibitor Cocktail (Roche). The addition of iodoacetamide was critical to reduce the formation of KCC2 containing high-molecular weight aggregates. Lysates were incubated 30 min at 4°C with rotation and centrifuged 1200g 5 min to remove debris. Total protein concentrations were determined with the micro BCA protein assay kit (*Pierce*) using the bovine serum albumin (BSA, Sigma-Aldrich) as a standard. The same day lysates were dissolved in Laemmli buffer (2% SDS, 20% glycerol, 5% β-mercaptoethanol, 62.5 mM TrisHCl and pH 7), pre-heated to 95˚C and directly loaded to a SDS-PAGE gel (Bolt 4-12% Bis-Tris Plus precast gels, Thermo Fisher Scientific, 20 ug of protein per lane). After transferring the proteins onto a nitrocellulose membrane (Thermo Scientific), the blots were probed first with chicken anti-KCC2 antibody (KCC2$_{chk}$, dilution 1:4000), recognizing the *N*-

terminus of the transporter (Markkanen et al., 2014) and revealed with anti-chicken Horseradish Peroxidase (HRP)-conjugated antibodies (1:3000, Life Technologies). Thereafter, the secondary antibody was stripped by 3 min incubation at 22°C with Restore PLUS Western Blot Stripping Buffer (Thermo Fisher Scientific) and membranes were probed with mixture of anti-KCC2 antibody ($KCC2_{rab}$), recognizing the *C*-terminus of the transporter (dilution 1:5000; US Biological, Euromedex, France) and mouse anti-α-tubulin antibody (α-tub, 1:3000, Thermo Fisher Scientific). The secondary antibodies were anti-rabbit Horseradish Peroxidase (HRP)-conjugated (1:3000, Life Technologies) and anti-mouse Cy3-conjugated immunoglobulins (1:2000; Jackson ImmunoResearch Laboratories). The chemiluminescent HRP Substrate (Immobilon, WBKLS0500, Millipore) was used to reveal HRP. All chemiluminescence and fluorescence signals were visualized with G:BOX gel imaging system (Syngene) and Genesys software.

Membrane biotinylation assay – N2a cells were plated on 60 mm cell culture dishes 24 h before transfection to obtain 80% of confluence at the day of transfection. Transfections with 5 µg per dish of DNA encoding KCC2, ΔNTD-KCC2, ΔCTD-KCC2 or pcDNA3.1 (mock) were performed using Lipofectamine 2000 according to manufacturer's protocol. 36 h after transfection, the cells were gently rinsed with phosphate-buffered saline (PBS) complemented with 0.1 mM $CaCl_2$ and 1 mM $MgCl_2$ (PBS/Ca/Mg) and incubated at 20°C with 2 mg/ml of EZ-Link Sulfo-NHS-SS-Biotin (21945, Thermo Scientific, USA) in PBS/Ca/Mg for 30 min. The reaction was quenched using PBS/Ca/Mg + 100 mM lysine (diluted with water to the final osmolarity of 300 mOsm). The cells were then rinsed 3 times with PBS/Ca/Mg and lysed in ice-cold RIPA lysis buffer. Lysates were incubated 30 min at 4°C with rotation, centrifuged 1200g 5 min to remove debris. Total protein concentrations were determined with the micro BCA protein assay kit (*Pierce*) using the bovine serum albumin (BSA, Sigma-Aldrich) as a standard. 20 ug of protein were collected and stored overnight at 4˚C (to maintain the same temperature regime as the fraction that was used for biotinylation process). 100 ug of protein were incubated with streptavidin-conjugated agarose (20347, Thermo Scientific, USA) overnight at 4˚C with rotation. The next day the agarose with bound biotinylated membrane proteins was washed 3 times with ice-cold RIPA buffer and one time with ice-cold PBS. Biotin-labeled proteins were eluted in a 50 µL of Laemmli buffer pre-heated to 95˚C (2% SDS, 20% glycerol, 5% β-mercaptoethanol, 62.5 mM TrisHCl and pH 7) and the entire volume was directly loaded to a SDS-PAGE gel. The described protocol includes important details that were experimentally elaborated to decrease the amount of biotin leakage from the intracellular environment. They include gentle rinsing of cells, incubation temperature at 20°C (but not 4°C) and the use of lysine instead of glycine for biotin quenching.

Analysis of western blots –In agreement with previous reports (Blaesse et al., 2006; Medina et al., 2014; Friedel et al., 2015), the SDS-PAGE and western blot analysis of KCC2 and its mutants revealed a

multi-band pattern of transporter migration. The bottom band reflected migration of the monomeric form of the protein whereas upper band(s) were agglomerates presumably containing oligomers and protein complexes formed by interaction with other proteins. The molecular weight of KCC2 and its mutants was estimated based on the migration of the monomeric band, whereas for quantitative analysis of the total protein expression, the intensity of the entire signal (monomer + agglomerates) was taken into account as it was previously described (Friedel et al., 2015). As a negative control, we used lysates of cells transfected with pcDNA3.1 (mock). Band intensities were quantified using Metamorph software.

For the biotinylation experiments, the endogenous transmembrane α-transferrin receptor was used as a loading control for both total cell lysates and biotinylated extracts. The amounts of total and biotinylated loaded fractions were adjusted to obtain approximately similar intensity of WT-KCC2 bands. The intracellular endogenous α-tubulin served as a control of biotin leakiness. The results were quantified as the ratio of biotinylated/total protein for each KCC2-related construct, α-transferrin receptor and α-tubulin.

Statistical analysis – Statistical analysis were conducted with OriginPro 9.0.0 which also indicated that assumptions of normality (Shapiro-Wilk test) and equal variance (Brown-Forsyth test) were met. A $p<0.05$ was considered significant for these and all subsequent tests. For data displaying normal distribution one-way ANOVA and the post hoc Tukey test were used for multiple comparisons between groups. For data displaying non-normal distribution, or experiments with a low number of independent replicates ($n<7$), Mann–Whitney U-test was used for comparison between 2 independent groups and Wilcoxon matched pairs test was employed to compare paired data.

RESULTS

Cellular expression of KCC2-pH$_{ext}$ – related constructs – To study the role of KCC2 intracellular domains in cell surface expression of the transporter, we generated KCC2 fusion proteins, where a pHluorin tag was inserted into the second putative extracellular loop of KCC2 protein (KCC2-pH$_{ext}$), and either the *N*- or *C*-termini of the protein was deleted (ΔNTD-KCC2-pH$_{ext}$ and ΔCTD-KCC2-pH$_{ext}$, respectively, Figure 1*A*). Tagging a membrane protein is challenging and problems can occur ranging from protein instability, misfolding, aberrant post-translational modifications, and functional changes (Maue, 2007). Thus, we first verified the protein expression level of the KCC2-related constructs. Whole cell extracts from N2a cells, transiently transfected with either KCC2-pH$_{ext}$, ΔNTD-KCC2-pH$_{ext}$ or ΔCTD-KCC2-pH$_{ext}$, were analyzed by western blotting using denaturing conditions (Figures 1*B-D*). For comparison, we

used a non-tagged wild-type KCC2 and the respective deleted mutants, ΔNTD-KCC2 and ΔCTD-KCC2.

The upper panel in Figure 1*B* shows a representative western blot of ΔNTD-KCC2, ΔNTD-KCC2-pH_{ext}, KCC2 and KCC2-pH_{ext}, visualized using a polyclonal antibody that recognizes an epitope located in the *C*-terminus region of the transporter (anti-$KCC2_{rab}$). A multiple band migration pattern was detected, where the bottom band corresponds to the monomeric state of the transporter (Figure 1*B*, ~140 kDa, indicated with an arrow), whereas the upper bands account for oligomers or high molecular weight protein complexes that were resistant to denaturing conditions (> 280 kDa). This migration pattern was already described previously and is typical for the KCC2 transporter (Blaesse et al., 2006; Medina et al., 2014; Friedel et al., 2015). The insertion of the pHluorin tag in KCC2 protein (KCC2-pH_{ext}) produced an expected 28 kDa increase in molecular weight of the monomer band and a similar upward shift of the oligomer/protein complexes migration (Figure 1*B*). The pattern of migration, the ratio monomer/total protein and the relative amount of total protein expression were similar for KCC2-pH_{ext} and non-tagged KCC2 (Figure 1*B, C*, *D* and Table 1).

The deletion of the *N*-terminus region in non-tagged KCC2 protein (ΔNTD-KCC2) resulted in an expected downward shift of both the monomer band (predicted molecular weight = 128 kDa) and the oligomer/protein complexes bands compared to wild-type KCC2 (Figure 1*B*). The insertion of the pHluorin tag in ΔNTD-KCC2 (ΔNTD-KCC2-pH_{ext}) provoked a positive shift in the molecular weight of the monomer band (up to 146 kDa, Figure 1*B*). Remarkably, we observed that in all experiments, the monomer band of ΔNTD-KCC2 (with or without tag) was barely detectable while the majority of ΔNTD-KCC2 proteins was concentrated in high molecular weight complexes. Although the total amount of ΔNTD-KCC2 and ΔNTD-KCC2-pH_{ext} protein expression did not differ from those of wild-type KCC2, we quantified a significant decrease in the ratio monomer/total compare to the wild-type KCC2 (Figure 1*C, D,* Table 1). Therefore, the deletion of the *N*-terminus of KCC2 does not perturb the protein translation, but significantly enhances the ability of the transporter to form multimolecular complexes resistant to denaturing conditions.

The lower panel of Figure 1*B* illustrates the migration pattern of KCC2, KCC2-pH_{ext}, ΔCTD-KCC2 and ΔCTD-KCC2-pH_{ext} visualized on the same western blot but using a polyclonal antibody that recognizes an epitope localized on the *N*-terminus domain of the transporter (anti-$KCC2_{chk}$). The monomer band of ΔCTD-KCC2 migrated close to the predicted position of 71 kDa (Figure 1*B*) and the ratio monomer/total protein did not statistically differ from those of wild-type KCC2 (Figure 1*B, C,* Table 1). Although, the high molecular weight complexes of ΔCTD-KCC2 exhibited smear-like migration pattern, whose aspect varied from one experiment to another (compare Figures 1*B* and 7*B*), the total intensity of ΔCTD-KCC2 protein did not differ from those of wild-type KCC2 (Figure 1*B*, *D*, Table 1). The insertion

of a pHluorin tag into ΔCTD-KCC2 protein produced an upward shift of both monomer and oligomer/protein complexes (ΔCTD-KCC2-pH_{ext}, Figure 1*B*) with a similar smear-like pattern for the high molecular complex. The consistency of molecular weight for ΔCTD-KCC2 monomer bands suggests that the mutant was correctly transcribed and translated. However, the deletion of the *C*-terminus formed a smear-like migration pattern for the high molecular complexes.

Next, to assess the subcellular distribution of created mutants, we transfected cultured hippocampal neurons with a mixture of plasmids encoding KCC2-pH_{ext} – derived constructs and mCherry, to visualize the neuron morphology (Figure 1*D*). Both ΔNTD-KCC2-pH_{ext} and ΔCTD-KCC2-pH_{ext} mutants were expressed in form of clusters in the soma, proximal and distal dendrites. The total intensity of fluorescence emitted by ΔNTD-KCC2-pH_{ext} and ΔCTD-KCC2-pH_{ext} neurons and normalized to the fluorescence of mCherry was not statistically different from those of wild-type KCC2-pH_{ext} (Figure 1*E*, *F* and Table 1). Similarly, there was no statistically significant difference in the relative level of mutants expression in proximal dendrites (Figure 1*E, G* and Table 1). However, the relative amount of protein expression in distal dendrites was twofold lower for ΔNTD-KCC2-pH_{ext} (p=5.8e-4, Mann-Whitney U-test, Figure 1*E, G,* Table 1) and higher for ΔCTD-KCC2-pH_{ext} (p=0.04, Mann-Whitney U-test, Figure 1*E, G* and Table 1) compared both to KCC2-pH_{ext}.

In overall, the insertion of a pHluorin tag in the extracellular loop of KCC2 mutants did not disturb the biochemical properties of the proteins compare to their non-tagged homologues. Although the deletion of either *N*- or *C*-termini of KCC2 did slightly perturb the migration pattern of the proteins as well as their distal dendrites localization, the proteins are effectively transcribed, translated and expressed in neurons.

Functionality of KCC2-pH_{ext} – To examine whether the insertion of the pHluorin tag may compromise KCC2 function, we coexpressed the KCC2-pH_{ext} with glycine receptor-channels (GlyR) in N2a cells and recorded the reversal potential of GlyR (EGly), which is principally determined by $[Cl^-]_i$, using gramicidin-perforated patch-clamp technique. The cells expressing KCC2-pH_{ext} were recognized through the weak fluorescence emitted by the pHluorin. For comparison we used cells expressing eGFP only (mock) and cells expressing non-tagged KCC2 subcloned in pIRES-GFP vector (Chudotvorova et al., 2005). Figure 2*A* shows an example of recording obtained for a KCC2-pH_{ext} or mock-transfected cell. We found that the $[Cl^-]_i$ calculated from EGly using the Nernst equation was much lower in KCC2-pH_{ext} expressing cells than in mock-transfected cells (statistically significant difference, p=0, Table 1) and was similar to the one recorded in cells expressing non-tagged KCC2 (p=0.89, Figure 2*B,* Table 1). This data indicated that KCC2-pH_{ext} overexpressed in heterologous expression system was functional and did not differ from non-tagged KCC2 in its ability to extrude Cl^-.

In its native neuronal environment, KCC2 interacts at least with 8 partners (Medina et al., 2014); some of them are neuron-restricted and control KCC2 activity (*e.g.*, Neto2, Ivakine et al., 2013)). To

assess if KCC2-pH$_{ext}$ is active when expressed in neurons, we overexpressed the construct in cultured immature hippocampal neurons at developmental stage 8-9 days *in vitro* (d.i.v.) characterized by low functional activity of endogenous KCC2 and relatively high level of $[Cl^-]_i$ (Chudotvorova et al., 2005; Pellegrino et al., 2011; Friedel et al., 2015). The measurements of the reversal potential of Cl^- permeable $GABA_A$ receptor-channel ($GABA_AR$) responses revealed statistically significant decrease of $[Cl^-]_i$ in neurons expressing KCC2-pH$_{ext}$ compared to mock-transfected neurons (Figure 2*C,* Table 1). $[Cl^-]_i$ in neurons expressing KCC2-pH$_{ext}$ was indistinguishable from the one measured in neurons transfected with non-tagged KCC2. Thus, KCC2-pH$_{ext}$ effectively reduces $[Cl^-]_i$ when expressed in either heterologous expression system or cultured hippocampal neurons.

Surface labeling of KCC2-pH$_{ext}$ mutants with deleted intracellular regions – Next we assessed the abundance of KCC2-pH$_{ext}$, ΔNTD-KCC2-pH$_{ext}$ and ΔCTD-KCC2-pH$_{ext}$ in different cell compartments of 13 d.i.v. hippocampal neurons using the previously described live-cell surface protein immunolabeling protocol (Figure 3*A*, Friedel et al., 2015). Namely, we labeled the extracellular tag of KCC2-pH$_{ext}$ using polyclonal rabbit anti-GFP antibody during 2 hours on living neurons and under normal culturing conditions (37°C, 5% CO_2). Presumably, at the end of this procedure, some of the labeled molecules remained on the cell surface, whereas others were internalized. The labeled molecules that were retained on the cell surface were visualized using secondary Cy3 conjugated anti-rabbit antibody applied to the living cells at low temperature (13°C), to prevent further protein internalization; the resulting fluorescence was identified as membrane fluorescence (F_m). This live-cell labeling protocol revealed small (<0.5 μm) and distinct clusters of different intensity that were restricted to the cell surface, as it is illustrated with images taken at different Z-plane (Figure 3*A* and 1st raw images in Figure 3*B*). These clusters resembled by their form and size to the live-cell labeled clusters of another KCC2 construct harboring 3xFlag as an extracellular tag (Chamma et al., 2013). The second pool of molecules, corresponding to KCC2-pH$_{ext}$ labeled and internalized, was visualized after post-hoc fixation of the same cells and additional labeling with Alexa-647 conjugated anti-rabbit antibody. The obtained Alexa-647 emitted fluorescence signal was mainly restricted to the intracellular compartments, but also revealed partially the Cy3-positive clusters retained on the cell surface (Figure 3*A* and 2nd raw images in Figure 3*B*). The "pure" internalized pool of fluorescence (F_i) was then obtained after arithmetic subtraction of Alexa-647 and Cy3 images (Figure 3*A* and 4th raw images in Figure 3*B*). To quantify the total amount of overexpressed KCC2-pH$_{ext}$, neurons were then labeled with mouse monoclonal anti-GFP antibody and revealed using Alexa-488 conjugated antibody (F_t, total fluorescence intensity, 3rd raw images in Figure 3*B*). The specificity of KCC2-pH$_{ext}$–related constructs surface labeling was verified using eGFP-KCC2 construct that carried a tag linked to the intracellular *N*-terminus of KCC2. The surface immunolabelling of neurons expressing eGFP-KCC2 did not reveal regularly distributed Cy3 or Alexa-647 positive clusters. Only rare clusters of significantly

weaker fluorescence intensity contributed to formation of the background signal (Figure 4*A*, 2nd images raw).

Although the four tested constructs (KCC2-pH$_{ext}$, ΔNTD-KCC2-pH$_{ext}$, ΔCTD-KCC2-pH$_{ext}$ and eGFP-KCC2) were well expressed into neurons and showed similar intensities of F_t, the amount of surface labelled fluorescent clusters strongly varied depending on the expressed molecule (Figure 4*A, B* and Table 2). Unlike neurons expressing wild-type KCC2-pH$_{ext}$, the cells with ΔNTD-KCC2-pH$_{ext}$ mutant were not decorated with bright puncta, resulting in a significantly lower F_m (Figure 4*A, B* and Table 2). The brightness and density of rare fluorescent F_m clusters detected on ΔNTD-KCC2-pH$_{ext}$ neurons were significantly smaller than those of KCC2-pH$_{ext}$ and were reminiscent to those characterizing the background staining of control neurons with eGFP-KCC2 (Figure 4*C* and Table 2). As consequence, the population data describing intensity of F_m signal in individual neurons were significantly lower in ΔNTD-KCC2-pH$_{ext}$, as compared to KCC2-pH$_{ext}$ and did not differ from eGFP-KCC2-transfected cells (Figure 4*B*, plot F_m and Table 2). Contrary to ΔNTD-KCC2-pH$_{ext}$, the neurons expressing ΔCTD-KCC2-pH$_{ext}$ construct had clearly detectable clusters located in the plasma membrane (Figure 4*A*, 4th images raw). The density of these clusters was similar to the one visualized on neurons with wild-type KCC2-pH$_{ext}$, but their brightness was statistically significantly weaker (Figure 4*C*, Table 2). The intensity of F_m emitted by ΔCTD-KCC2-pH$_{ext}$ neurons was significantly lower as compared to wild-type KCC2-pH$_{ext}$, but was significantly higher as compared to ΔNTD-KCC2-pH$_{ext}$ neurons and control eGFP-KCC2-positive cells (Figure 4*B*, plot F_m, Table 2).

The decreased surface expression of ΔNTD-KCC2-pH$_{ext}$ and ΔCTD-KCC2-pH$_{ext}$ mutants could be the result of reduced surface delivery of the molecules or enhanced internalization processes. Analysis of the fluorescence intensity of immunelabeled and internalized clusters revealed no detectable F_i signal in neurons expressing ΔNTD-KCC2-pH$_{ext}$ mutant (Figure 4*A*, *B*), and thus, indicated that the deletion of *N*-terminus prevented delivery of the KCC2 into the plasma membrane. In contrast to neurons with ΔNTD-KCC2-pH$_{ext}$, the cells expressing ΔCTD-KCC2-pH$_{ext}$ construct exhibited more than 10-fold higher rate of internalization (statistically significant difference, p=2.86e^{-6}, Figure 4*B* plot F_i and Table 2).

The decreased surface delivery of ΔNTD-KCC2-pH$_{ext}$ mutant was further confirmed in another set of experiments with modified live staining protocol (see materials and methods for details) designed to visualize all molecules labeled on the cell surface during a 2-hour period (Figure 4*D*). Any labelled clusters were detected on ΔNTD-KCC2-pH$_{ext}$ positive neurons; the median value of F_{all} signal measured on ΔNTD-KCC2-pH$_{ext}$ cells was more than 20-fold lower than that of wild-type KCC2-pH$_{ext}$ neurons (0.04 and 0.92, respectively, p=2.64e^{-13}, Figure 4*D* and Table 2). Moreover the distribution of the F_{all} values in ΔNTD-KCC2-pH$_{ext}$ neurons was similar to the one measured in eGFP-KCC2-positive cells (non-significant difference, p=0.2, Figure 4*D* and Table 2). Contrary to ΔNTD-KCC2-pH$_{ext}$, the F_{all} signal in

ΔCTD-KCC2-pH_{ext} positive neurons was well detectable and was even significantly stronger than the one in wild-type KCC2-pH_{ext} (correspondent medians were 1.45 and 0.92, $p=9.56e^{-4}$, Figure 4*D* and Table 2). We concluded, therefore, that the deletion of the *N*-terminus of KCC2-pH_{ext} fully abolished plasmalemmal delivery of the protein, whereas construct composed only of the *N*-terminus and transmembrane regions was well delivered to the cell surface. Once expressed into the plasma membrane, ΔCTD-KCC2-pH_{ext} proteins were rapidly internalized, which accounted for the 2-fold lower amount of F_m and higher amount of F_i as compared to wild-type KCC2-pH_{ext}. Taken together these data indicated that *N*-terminus is indispensable for surface delivery of KCC2-pH_{ext}.

Surface expression of KCC2-pH_{ext} mutants in heterologous cell lines – The neuronal environment is crucial for KCC2 function and regulation and Li et al. (Li et al., 2007) found that ΔNTD-KCC2 was expressed in the plasma membrane of HEK293 cells. Therefore, we then asked whether the surface delivery of ΔNTD-KCC2-pH_{ext} mutant is also compromised in cell lines. We examined the expression of non-mutated KCC2-pH_{ext}, ΔNTD-KCC2-pH_{ext} and ΔCTD-KCC2-pH_{ext} mutants in two different cell lines; neuron-derived N2a and non-neuronal HEK293 cells.

Similarly to neurons, we found that in both cell lines the deletion of the *N*-terminus of KCC2-pH_{ext} fully abolished the mutant's surface expression, whereas the ΔCTD-KCC2-pH_{ext} construct composed of *N*-terminus and transmembrane regions was well labeled on the cell surface (Figure 5*A*). The relative intensities of F_m and F_i signals in HEK293 and N2a cell lines expressing ΔCTD-KCC2-pH_{ext} mutant resembled those analyzed in neurons (Figure 5*B* and Table 3). We concluded therefore, that the *N*-terminus is essential for the plasmalemmal delivery of KCC2-pH_{ext} regardless the expression system. Of note, we found that wild-type KCC2-pH_{ext} was labeled on the cell surface of 98% of studied neurons, 99% of N2a cells but only 62% of HEK293 cells (Figure 6), indicating a possible difference in the mechanisms controlling KCC2 surface delivery in N2a and HEK293 cell lines.

Biotinylation of KCC2 mutants – To exclude a possible contribution of the extracellular tag to the mutant surface delivery and internalization, we analyzed the surface expression of non-tagged wild-type KCC2, ΔNTD-KCC2 and ΔCTD-KCC2 proteins using biotinylation assay in N2a cells followed by SDS/PAGE separation and western blotting (Figure 7). As in the western blot analysis depictured in Figure 1, the expression of ΔNTD-KCC2 mutant was visualized using anti-$KCC2_{rab}$ antibody recognizing the *C*-terminus of KCC2 (Figure 7*A*) whereas the expression of ΔCTD-KCC2 mutant was detected with anti-$KCC2_{chk}$ antibody recognizing the *N*-terminus of the transporter (Figure 7*B*). In the same samples, we characterized also the cellular expression and surface biotinylation level of the transmembrane α-transferrin receptor (α-tr) and the cytoplasmic α-tubulin (α-tub). α-tr labeling was used as a positive control for the biotinylation efficacy and loading of total and biotinylated protein fractions. α-tub, an intracellular protein that should not be biotinylated, was used as a negative control to determine the level

of inevitable leakage of the biotinylation compound into the intracellular environment. A special attention was attributed to the improvement of the experimental protocol with the final purpose of decreasing biotin leakage (see materials and methods for details). We quantified the intensity of each bands and expressed the results as the ratio of biotinylated/total protein for α-tr, α-tub and KCC2 (Figure 7*C-D*). As illustrated in Figure 7A and quantified in Figure 7*C*, the biotinylated/total protein ratio was significantly lower in neurons expressing ΔNTD-KCC2 compared to the one in neurons expressing WT-KCC2. Moreover, consistent with experiments involving ΔNTD-KCC2-pH_{ext} (Figure 5), the biotinylation level of ΔNTD-KCC2 was indistinguishable from the one of leakage biotinylation revealed using α-tub antibody (p=0.69, Figure 7*C* and Table 4). Contrary to ΔNTD-KCC2 mutant, the level of the surface labeling of ΔCTD-KCC2 mutant was not statistically different from the labeling of WT-KCC2 (p=0.92 Figure 7*B* and Table 4) and was significantly higher than the level of surface unrelated labeling of α-tub in the same cell sample (p=0.02, Figure 7*D* and Table 4). We concluded therefore that the truncation of the *N*-terminus of naïve KCC2 prevented plasmalemmal expression of the transporter, whereas the truncation of the *C*-terminus did not affect this process.

DISCUSSION

In the present work, we demonstrated that KCC2-pH_{ext} is a suitable and useful tool to assess the membrane expression of exogenous KCC2 proteins in neurons and heterologous systems. We found that the *N*-terminus is required for KCC2 insertion into the plasma membrane, regardless of the expression system, while the *C*-terminus is critical for the membrane stability of KCC2. Our results suggest that cargo proteins responsible for KCC2 trafficking to the plasma membrane are interacting with regions other than *C*-terminus and highlight the *N*-terminus of KCC2 as a critical element for this mechanism (Figure 8).

We took advantage of the KCC2-pH_{ext} construct to analyze the role of the intracellular tails for the plasma membrane expression and internalization of KCC2. While questions about the role of diverse mutations and structural elements on KCC2 surface expression are of primary importance, the relatively low percentage of endogenous KCC2 expressed at the plasma membrane and the absence of specific antibody recognizing extracellular domains of the transporter make these questions challenging. To circumvent these limitations, a number of KCC2 chimera with tags in the extracellular loops were created and successfully used to characterize the surface expression of different mutants (Zhao et al., 2008; Acton et al., 2012; Chamma et al., 2013; Weber et al., 2014). Along this line, KCC2-pH_{ext}, was previously employed to characterize the surface expression of KCC2 mutants associated with human idiopathic generalized epilepsy (Kahle et al., 2014) and describe the functional significance of KCC2's Thr906 and

Thr1007 phosphorylation sites (Friedel et al., 2015). In the present study, we performed a detailed analysis of the biochemical and biophysical properties of KCC2-pH_{ext}. We demonstrated that the insertion of the pHluorin tag does not affect the migration pattern of KCC2 and preserves its ion transport ability. More importantly, the pHluorin tag did not modify the migration pattern of mutants with deleted *N*- and *C*-termini and yielded discoveries about novel roles of intracellular tails in surface expression of KCC2.

Our main discovery is the critical role of the *N*-terminus for the surface delivery of KCC2. This finding was unexpected as previous study illustrated the effective biotinylation (*e.g*. surface expression) of ΔNTD-KCC2 in HEK293 cells (Li et al., 2007). The cited work was, however, *qualitative* and did not provide *quantitative* analysis with taking into account controls of the biotin leakiness in cells expressing KCC2 and ΔNTD-KCC2. So far, no other studies were performed to address the question of the role of *N*-terminus for proper surface delivery of the KCC2. We have found that decreased surface expression of ΔNTD-KCC2-pH_{ext} mutant is the result of perturbed protein surface delivery, whereas decreased surface expression of ΔCTD-KCC2-pH_{ext} mutant is consequent to an enhanced protein internalization rate. These results were further confirmed using a biotinylation approach and non-tagged KCC2 constructs.

What are the clues to explain the default of ΔNTD-KCC2 expression at the plasma membrane? Our results showing the expected molecular weight of the monomeric form of ΔNTD-KCC2 mutant suggest that the protein is at least correctly translated and are consistent with a previous study (Horn et al., 2010). Also, the authors found that ΔNTD-KCC2 interacts with the neuronal cytoskeleton associated protein 4.1N similarly to the wild-type KCC2 and therefore suggested that ΔNTD-KCC2 mutant is correctly folded. In such case, one can suggests that the deletion of the *N*-terminus perturbs the interaction of KCC2 with surface-delivery machinery without affecting structural integrity of the mutant. However, our finding of the modified monomer/total protein ratio do not exclude possible modifications in the tertiary/quaternary structure of ΔNTD-KCC2 protein that could cause the mutant to be stacked at one of the multiple checkpoint of the secretory pathway. Future studies are required to characterize more in details the structural changes associated with the deletion of the *N*-terminus of KCC2.

We further highlighted the critical role of the *N*-terminus for KCC2 surface delivery using two constructs only composed of *N*-terminus and transmembrane regions (*i.e.* ΔCTD-KCC2-pH_{ext} and ΔCTD-KCC2 mutants). Both mutants were effectively inserted into the plasma membrane. This observation provides a novel perception on the structural role of *C*-terminus in KCC2's function and indicates that the *C*-terminal domain is not required for the surface insertion of the transporter. However, after effective delivery to the plasma membrane the ΔCTD-KCC2-pH_{ext} mutant was rapidly internalized suggesting an important role of *C*-terminus for KCC2 stabilization into the plasma membrane. An alternative explanation could be that because of a compromised structure and folding, the protein undergoes a rapid internalization to be further degraded. This suggestion is in agreement with the consistent observation of a

smear-like pattern of migration for ΔCTD-KCC2-pH_{ext} and ΔCTD-KCC2 mutants. Yet the mechanisms controlling the internalization and degradation of KCC2 are out of the scope of the present work and constitute a crucial subject for further studies.

The understanding of the structure-functional organization of KCC2 transporter is among first priorities in the field, as KCC2 is a putative target for development of therapeutic treatments (Kahle et al., 2013; Löscher et al., 2013; Medina et al., 2014). Up to date, most of reported functionally important KCC2's regulatory sites are located on the long intracellular *C*-terminus (Lee et al., 2007, 2010; Li et al., 2007; Rinehart et al., 2009; Acton et al., 2012; Kahle et al., 2014; Puskarjov et al., 2014; Weber et al., 2014). The structure-functional importance of the intracellular *N*-terminus of KCC2 is much less studied. A recent work suggested the importance of KCC2 *N*-terminus domain for the neuroprotection (Winkelmann et al., 2015). The *N*-terminus of KCC2 also carries several putative regulatory sites, including phosphorylatable serine residues (Weber et al., 2014) and the Ste20-related proline alanine-rich kinase/oxidative stress response-1 (SPAK/OSR1) binding motif (Uvarov et al., 2007); however their functional importance remains obscure. The present work provides an important clue for further research directed to describe the mechanisms of KCC2 surface insertion and the precise role of the *N*-terminus domain in this process. In addition to surface insertion mechanism, we have noticed the importance of the *N*-terminus for KCC2 expression into distal dendrites. Indeed, the truncation of the *N*-terminus of KCC2-pH_{ext} resulted in decreased dendritic expression of the transporter, whereas the construct composed of only the *N*-terminus and transmembrane domains showed two-fold higher dendritic expression. These results are in agreement with similar finding reported by Winkelmann et al. (Winkelmann et al., 2015). Although the identification of the mechanisms involved in the decreased expression of ΔNTD-KCC2 in the distal dendritic compartment was out of the scope in the present study, our findings highlight one more potential structure-function role for the *N*-terminus region that should be taken into account in future experimentations.

The KCC2 mutant with deleted *N*-terminus is widely used as a molecular tool in studies dedicated to characterize mechanisms of regulatory actions of KCC2 (Li et al., 2007; Bortone and Polleux, 2009; Horn et al., 2010; Gauvain et al., 2011; Fiumelli et al., 2013; Winkelmann et al., 2015). In particular, the experiments using ΔNTD-KCC2 mutant served as a key argument in the hypothesis of the structural (ion-transport independent) mechanism of KCC2's regulatory action (Li et al., 2007; Horn et al., 2010; Fiumelli et al., 2013). Our finding does not place in question this hypothesis, as ΔNTD-KCC2 possess the putative region on the *C*-terminus mediating the trophic action of KCC2 (Li et al., 2007) and overexpression of only intracellular *C*-terminus exerted the similar regulatory action (Fiumelli et al., 2013); however, it should be considered for future works suggesting proper dendritic delivery and surface expression of the transporter.

In conclusion, our results support a novel view on the role of the *N*-terminus domain in the control of KCC2 surface expression. As KCC2 is a putative target for novel therapeutic treatments, our finding highlights the *N*-terminus as a crucial target for strategies designed to enhance KCC2's surface delivery.

REFERENCES

Acton B a, Mahadevan V, Mercado A, Uvarov P, Ding Y, Pressey J, Airaksinen MS, Mount DB, Woodin M a (2012) Hyperpolarizing GABAergic transmission requires the KCC2 C-terminal ISO domain. J Neurosci 32:8746–8751.

Blaesse P, Airaksinen MS, Rivera C, Kaila K (2009) Cation-chloride cotransporters and neuronal function. Neuron 61:820–838.

Blaesse P, Guillemin I, Schindler J, Schweizer M, Delpire E, Khiroug L, Friauf E, Nothwang HG (2006) Oligomerization of KCC2 correlates with development of inhibitory neurotransmission. J Neurosci 26:10407–10419.

Bortone D, Polleux F (2009) KCC2 expression promotes the termination of cortical interneuron migration in a voltage-sensitive calcium-dependent manner. Neuron 62:53–71.

Buerli T, Pellegrino C, Baer K, Lardi-Studler B, Chudotvorova I, Fritschy J-M, Medina I, Fuhrer C (2007) Efficient transfection of DNA or shRNA vectors into neurons using magnetofection. Nat Protoc 2:3090–3101.

Chamma I, Chevy Q, Poncer JC, Lévi S (2012) Role of the neuronal K-Cl co-transporter KCC2 in inhibitory and excitatory neurotransmission. Front Cell Neurosci 6:5.

Chamma I, Heubl M, Chevy Q, Renner M, Moutkine I, Eugene E, Poncer JC, Levi S (2013) Activity-Dependent Regulation of the K/Cl Transporter KCC2 Membrane Diffusion, Clustering, and Function in Hippocampal Neurons. J Neurosci 33:15488–15503.

Chudotvorova I, Ivanov A, Rama S, Hübner C a, Pellegrino C, Ben-Ari Y, Medina I (2005) Early expression of KCC2 in rat hippocampal cultures augments expression of functional GABA synapses. J Physiol 566:671–679.

571 Fiumelli H, Briner A, Puskarjov M, Blaesse P, Belem BJ, Dayer AG, Kaila K, Martin J-L, Vutskits L
572 (2013) An Ion Transport-Independent Role for the Cation-Chloride Cotransporter KCC2 in Dendritic
573 Spinogenesis In Vivo. Cereb Cortex 23:378–388.
574 Friedel P, Kahle KT, Zhang J, Hertz NT, Pisella LI, Buhler E, Schaller F, Duan J, Khanna AR, Bishop
575 PN, Shokat KM, Medina I (2015) WNK1-regulated inhibitory phosphorylation of the KCC2
576 cotransporter maintains the depolarizing action of GABA in immature neurons. Sci Signal 8:23–26.
577 Gauvain G, Chamma I, Chevy Q, Cabezas C, Irinopoulou T, Bodrug N, Carnaud M, Lévi S, Poncer JC
578 (2011) The neuronal K-Cl cotransporter KCC2 influences postsynaptic AMPA receptor content and
579 lateral diffusion in dendritic spines. Proc Natl Acad Sci U S A 108:15474–15479.
580 Horn Z, Ringstedt T, Blaesse P, Kaila K, Herlenius E (2010) Premature expression of KCC2 in embryonic
581 mice perturbs neural development by an ion transport-independent mechanism. Eur J Neurosci
582 31:2142–2155.
583 Ivakine EA, Acton BA, Mahadevan V, Ormond J, Tang M, Pressey JC, Huang MY, Ng D, Delpire E,
584 Salter MW, Woodin MA, McInnes RR (2013) Neto2 is a KCC2 interacting protein required for
585 neuronal Cl- regulation in hippocampal neurons. Proc Natl Acad Sci U S A 110:3561–3566.
586 Kahle KT et al. (2014) Genetically encoded impairment of neuronal KCC2 cotransporter function in
587 human idiopathic generalized epilepsy. EMBO Rep 15:766–774.
588 Kahle KT, Deeb TZ, Puskarjov M, Silayeva L, Liang B, Kaila K, Moss SJ (2013) Modulation of neuronal
589 activity by phosphorylation of the K-Cl cotransporter KCC2. Trends Neurosci 36:726–737.
590 Lee HHC, Jurd R, Moss SJ (2010) Tyrosine phosphorylation regulates the membrane trafficking of the
591 potassium chloride co-transporter KCC2. Mol Cell Neurosci 45:173–179.
592 Lee HHC, Walker J a, Williams JR, Goodier RJ, Payne J a, Moss SJ (2007) Direct protein kinase C-
593 dependent phosphorylation regulates the cell surface stability and activity of the potassium chloride
594 cotransporter KCC2. J Biol Chem 282:29777–29784.
595 Li H, Khirug S, Cai C, Ludwig A, Blaesse P, Kolikova J, Afzalov R, Coleman SK, Lauri S, Airaksinen
596 MS, Keinänen K, Khiroug L, Saarma M, Kaila K, Rivera C (2007) KCC2 interacts with the dendritic

cytoskeleton to promote spine development. Neuron 56:1019–1033.

Löscher W, Puskarjov M, Kaila K (2013) Cation-chloride cotransporters NKCC1 and KCC2 as potential targets for novel antiepileptic and antiepileptogenic treatments. Neuropharmacology 69:62–74.

Markkanen M, Karhunen T, Llano O, Ludwig A, Rivera C, Uvarov P, Airaksinen MS (2014) Distribution of neuronal KCC2a and KCC2b isoforms in mouse CNS. J Comp Neurol 522:1897–1914.

Maue RA (2007) Understanding ion channel biology using epitope tags: progress, pitfalls, and promise. J Cell Physiol 213:618–625.

Medina I, Friedel P, Rivera C, Kahle KT, Kourdougli N, Uvarov P, Pellegrino C (2014) Current view on the functional regulation of the neuronal K+-Cl− cotransporter KCC2. Front Cell Neurosci 8:1–18.

Payne JA, Stevenson TJ, Donaldson LF (1996) Molecular characterization of a putative K-Cl cotransporter in rat brain. A neuronal-specific isoform. J Biol Chem 271:16245–16252.

Pellegrino C, Gubkina O, Schaefer M, Becq H, Ludwig A, Mukhtarov M, Chudotvorova I, Corby S, Salyha Y, Salozhin S, Bregestovski P, Medina I (2011) Knocking down of the KCC2 in rat hippocampal neurons increases intracellular chloride concentration and compromises neuronal survival. J Physiol 589:2475–2496.

Puskarjov M, Seja P, Heron SE, Williams TC, Ahmad F, Iona X, Oliver KL, Grinton BE, Vutskits L, Scheffer IE, Petrou S, Blaesse P, Dibbens LM, Berkovic SF, Kaila K (2014) A variant of KCC2 from patients with febrile seizures impairs neuronal Cl- extrusion and dendritic spine formation. EMBO Rep 15:723–729.

Rinehart J, Maksimova YD, Tanis JE, Stone KL, Caleb A, Zhang J, Risinger M, Pan W, Wu D, Christopher M, Forbush B, Joiner CH, Gulcicek EE, Gallagher PG, Hodson C a, Colangelo CM, Lifton RP (2009) Sites of regulated phosphorylation that control K-Cl cotransporter activity. Cell 138:525–536.

Rivera C, Voipio J, Payne JA, Ruusuvuori E, Lahtinen H, Lamsa K, Pirvola U, Saarma M, Kaila K (1999) The K+/Cl- co-transporter KCC2 renders GABA hyperpolarizing during neuronal maturation. Nature 397:251–255.

623 Stein V, Hermans-Borgmeyer I, Jentsch TJ, Hübner C a (2004) Expression of the KCl cotransporter
624 KCC2 parallels neuronal maturation and the emergence of low intracellular chloride. J Comp Neurol
625 468:57–64.
626 Stödberg T et al. (2015) Mutations in SLC12A5 in epilepsy of infancy with migrating focal seizures. Nat
627 Commun 6:8038.
628 Tao R, Li C, Newburn EN, Ye T, Lipska BK, Herman MM, Weinberger DR, Kleinman JE, Hyde TM
629 (2012) Transcript-Specific Associations of SLC12A5 (KCC2) in Human Prefrontal Cortex with
630 Development, Schizophrenia, and Affective Disorders. J Neurosci 32.
631 Uvarov P, Ludwig A, Markkanen M, Pruunsild P, Kaila K, Delpire E, Timmusk T, Rivera C, Airaksinen
632 MS (2007) A novel N-terminal isoform of the neuron-specific K-Cl cotransporter KCC2. J Biol
633 Chem 282:30570–30576.
634 Weber M, Hartmann A-M, Beyer T, Ripperger A, Nothwang HG (2014) A novel regulatory locus of
635 phosphorylation in the C terminus of the potassium chloride cotransporter KCC2 that interferes with
636 N-ethylmaleimide or staurosporine-mediated activation. J Biol Chem 289:18668–18679.
637 Winkelmann A, Semtner M, Meier JC (2015) Chloride transporter KCC2-dependent neuroprotection
638 depends on the N-terminal protein domain. Cell Death Dis 6:e1799.
639 Woo N-S, Lu J, England R, McClellan R, Dufour S, Mount DB, Deutch AY, Lovinger DM, Delpire E
640 (2002) Hyperexcitability and epilepsy associated with disruption of the mouse neuronal-specific K-
641 Cl cotransporter gene. Hippocampus 12:258–268.
642 Zhao B, Wong AYC, Murshid A, Bowie D, Presley JF, Bedford FK (2008) Identification of a novel di-
643 leucine motif mediating K(+)/Cl(-) cotransporter KCC2 constitutive endocytosis. Cell Signal
644 20:1769–1779.
645

646 **FIGURE LEGENDS**

647 **FIGURE 1.** Biochemical properties and expression profile of KCC2-pH_{ext} and its mutants with truncated
648 *N*- and *C*-termini. *A, s*chematic drawings of KCC2-pH_{ext}, ΔNTD-KCC2-pH_{ext} and ΔCTD-KCC2-pH_{ext}.

649 The ΔNTD-KCC2-pH$_{ext}$ and ΔCTD-KCC2-pH$_{ext}$ mutants were created by deletion of the first 100 amino
650 acids and the last 470 amino acids from respectively the *N*- and *C*-termini of KCC2-pH$_{ext}$. *B*, western blot
651 of extracts from N2a cells overexpressing pcDNA3.1 (mock) and indicated KCC2-derived constructs.
652 Arrows indicate the location of the monomer band for each respective construct. The blot was first
653 revealed using anti-KCC2$_{chk}$ antibody recognizing KCC2's *C*-terminus domain and then using anti-
654 KCC2$_{rab}$ antibody raised against *N*-terminus of KCC2b and anti-α-tubulin antibody. Notice the weak
655 intensity of monomer band of ΔNTD-KCC2 and ΔNTD-KCC2-pH$_{ext}$ mutants. *C*, Tukey boxplots of the
656 calculated monomer/total protein ratio for each construct revealed using anti-KCC2$_{rab}$ (upper plot) and
657 anti-KCC2$_{chk}$ (bottom plot) antibodies. WT – wild-type KCC2; pH - KCC2-pH$_{ext}$; ΔN - ΔNTD-KCC2;
658 ΔN-pH - ΔNTD-KCC2-pH$_{ext}$; ΔC - ΔCTD-KCC2; ΔC-pH - ΔCTD-KCC2-pH$_{ext}$; 6 experiments. ***$p <$
659 0.001; *$p < 0.05$; non-parametric Wilcoxon matched pairs test. *D*, Tukey boxplots of the total expression
660 of KCC2-related constructs normalized to the intensity of endogenous α–tubulin. No statistically
661 significant difference was detected between wild-type KCC2 and each particular mutant. Non-parametric
662 Wilcoxon matched pairs test; 6 experiments (see Table 1 for the exact *p* values). *E*, representative images
663 of neurons transfected with mCherry and mentioned mutants of KCC2-pH$_{ext}$. The mCherry was expressed
664 to visualise the morphology of the neuron and was revealed using rabbit polyclonal anti-DsRed antibody
665 and Cy3-conjugated secondary antibody. The cellular expression of KCC2-pH$_{ext}$ was revealed using
666 mouse anti-GFP antibody and Alexa 488-conjugated secondary antibody. The fluorescent images of Alexa
667 488 were scaled for each neuron to obtain 90% of maximal intensity in brightest region and were false-
668 colored using rainbow Look-Up Table (LUT) shown on the left. The white rectangles indicate regions
669 where ROI were drawn and fluorescence intensities measured for quantification shown in *G*. The high
670 zoom images were taken on the distance between 150 and 200 µm from soma and illustrate KCC2-pH$_{ext}$
671 mutants' expression in secondary dendrites. Scale bars are 20 µm for left column images and 1 µm for
672 right column images. Notice that wild-type KCC2-pH$_{ext}$ as well as both mutants were expressed in the
673 soma and dendrites, including the tiny dendrite extremities, but the level of ΔNTD-KCC2-pH$_{ext}$ expression
674 was lower in distal dendrites. *F*, Quantification of GFP fluorescence intensity (normalized to mCherry) in
675 neurons expressing KCC2-pH$_{ext}$ (pH), ΔNTD-KCC2-pH$_{ext}$ (ΔN-pH) or ΔCTD-KCC2-pH$_{ext}$ (ΔC-pH).
676 Pooled data from 3 experiments, 4 neurons per experiment and condition. No statistical difference were
677 observed between conditions, Mann-Whitney U-test (see Table 1 for details). *G*, Quantification of GFP
678 fluorescence intensity in distal (upper panel, corresponding to region 1 in *E*) and proximal (lower panel,
679 corresponding to region 2 in *E*) dendrites of transfected neurons. The data were then normalized to the
680 fluorescence of a reference region "ref". Pooled data from 3 experiments, 4 neurons per experiment and
681 condition. *: $p<0.05$; ***: $p<0.001$, Mann-Whitney U-test (see Table 1 for details). For the boxplots, the
682 box extends from the first (Q1) to third (Q3) quartiles. The line and solid circle inside the box represent

683 median and mean, respectively. The whiskers define the outermost data point that falls within upper inner
684 and lower inner fence (Q1-1.5(IQR) and (Q3-1.5(IQR), respectively. Black dots show values of individual
685 measurements.
686
687 **FIGURE 2.** Recombinant KCC2-pH$_{ext}$ is functional. *A,* the traces show representative currents induced by
688 focal applications of glycine to N2a cells expressing KCC2-pH$_{ext}$ or eGFP (mock) at different voltage
689 steps. In the I-V plot GlyR-mediated current amplitudes were plotted against holding membrane potential.
690 The current intercepts the voltage axis at EGly (-41 mV and -89 mV for KCC2-pH$_{ext}$ and eGFP,
691 respectively). The numbers above interception points indicated quantified using Nernst equation $[Cl^-]_i$
692 values. *B*, Tukey boxplots of the calculated $[Cl^-]_i$ values measured as shown in *A* for N2a cells expressing
693 KCC2-pH$_{ext}$, eGFP (mock) or KCC2-IRES-GFP (KCC2). Pooled data from 4 cultures, 5–8 cells per
694 culture and condition. ***:$p < 0.001$, ns non-significant, one-way ANOVA and post-hoc Tukey test (see
695 Table 1 for details). *C*, the calculated $[Cl^-]_i$ from E_{GABAA} measurements in 8-9 d.i.v. neurons expressing
696 KCC2-pH$_{ext}$, eGFP (mock) or KCC2-IRES-GFP (KCC2). 8 cultures, 2–3 neurons per culture and
697 condition. **:$p < 0.01$, ns non-significant, one-way ANOVA test.
698
699 **FIGURE 3.** Visualization of surface expressed and internalized KCC2-pH$_{ext}$ proteins using a live-cell
700 immunolabelling protocol on cultured hippocampal neurons. *A,* scheme of the multistep immunolabeling
701 protocol applied to 13 d.i.v. neurons. 1st Ab, primary antibody; 2nd Cy3, Cy3-conjugated secondary
702 antibody; 2nd Alexa 647, Alexa-conjugated secondary antibody; PFA, paraformaldehyde. The scheme does
703 not include final steps of fixed and permeabilised cells labelling with mouse anti-GFP and anti-mouse
704 Alexa 488 antibody (total protein pool (F_t)). *B*, representative images showing fluorescence emitted after
705 staining with Cy3-conjugated secondary antibody (plasma membrane restricted pool (F_m); images were
706 pseudocolored using illustrated bi-color LUT, 1st raw); Alexa 647-conjugated secondary antibody
707 (internalized surface labelled molecules and portion of surface retained molecules, 2nd raw); Alexa 488-
708 conjugated secondary antibody (F_t, 3rd raw); internalized surface labelled signal obtained by arithmetic
709 subtraction of 1st and 2nd raw images (F_i, 4th raw). Image columns illustrate fluorescent signals obtained at
710 different Z-planes or after arithmetic summation of 9 planes as indicated. The neuronal shape (Alexa 488
711 fluorescence) is shown in light green in each image for reference. The insets illustrate indicated portion of
712 images at higher zoom. Scale bars: 8 µm in main image, 1 µm in inset.
713
714 **FIGURE 4.** Surface expression of KCC2-pH$_{ext}$ mutants with deleted intracellular *N*- and *C*-termini in
715 cultured hippocampal neurons. *A,* Schematic drawings of KCC2-pH$_{ext}$ mutants and representative images
716 showing fluorescence emitted after total protein staining (F_t), by plasma membrane restricted pool (F_m)

and internalized pool of labeled molecules (F_i). Images illustrate the fluorescence obtained after the summation of ten Z-planes acquired for each channel as described in Figure 3B. *B-D*, Summary data of indicated morphometric parameters characterizing surface expression of mutants (the values were normalized to mean KCC2-pH_{ext} in each experiment). The protocol used to determine the F_{all} depictured in panel *D* is described in materials and methods. Pooled data from 4 cultures, 4-8 neurons per culture and condition. ***, $p<0.001$, Mann-Whitney non-parametric test (see Table 2 for more details). Parameters of boxplots are the same as detailed in Figure 1.

FIGURE 5. Properties of wild-type KCC2-pH_{ext} (WT), ΔNTD- and ΔCTD-KCC2-pH_{ext} mutants are not restricted to neuronal environment. *A,* representative images of N2a cells showing total protein fluorescence (F_t), plasma membrane staining (F_m) and internalized fluorescence (F_i) of indicated constructs in the same experimental paradigm as depicted in Figure 4. Scale bar 20 µm. *B,* comparison of morphometric parameters characterizing surface expression of mentioned mutants in neurons, HEK293 and N2a cells. Plots showing mean ± SEM of indicated values that were normalized to KCC2-pH_{ext}. Pooled data from 4 experiments, 20-25 cells per experiment and condition. Statistical significance of differences between columns is shown in Table 1. Notice that, similarly to neurons, in both cell lines the deletion of the *N*-terminus of KCC2-pH_{ext} fully abolished the mutant's surface expression, whereas the deletion of the *C*-terminus facilitated the plasma membrane surface delivery. Once delivered to the plasma membrane, ΔCTD-KCC2-pH_{ext} mutants were rapidly internalized. As consequence, the amount of surface expressed ΔCTD-KCC2-pH_{ext} relative to wild-type KCC2-pH_{ext} was significantly lower in both HEK293 and N2a cells whereas internalized pool of the mutant was 7 to 15-fold stronger in these cells, respectively.

FIGURE 6. High variability in the surface expression of WT-KCC2-pH_{ext} in HEK293 cells. *A,* representative images of HEK293 cells illustrating variability in surface labeling of WT-KCC2-pH_{ext} (upper panel). While two HEK293 cells (indicated with arrowhead and arrow) show similar amounts of total expressed WT-KCC2-pH_{ext}, the level of surface labeled proteins differ in these cells. The bottom panel illustrates negative control surface labeling of eGFP-KCC2 construct with intracellularly located tag. *B,* distribution histograms characterizing surface labeling (F_{all}) of WT-KCC2-pH_{ext} protein expressed in neurons, HEK293 or N2a cells. Insets show the F_{all} distribution for the control eGFP-KCC2 construct. The dotted lines in insets reproduce the distribution profile of KCC2-pH_{ext} for comparison. Note that the distribution profile for HEK293 cells transfected with KCC2-pH_{ext} is different compared to neurons and N2a, with predominance of cells with low F_{all}. (6 experiments, 25 analyzed cells per experiment).

FIGURE 7. Surface biotinylation of non-tagged KCC2 mutants. *A*, representative Western blots of total extracts (left panel) and biotinylated fractions (right panel) of N2a cells transfected with wild-type KCC2 (WT), pcDNA3.1 (mock) and ΔNTD-KCC2 (ΔNTD). Detection with anti-KCC2 rabbit ($KCC2_{rab}$) antibody recognizing *C*-terminus of KCC2. Anti-α-transferrin receptor antibody (α-tr) and anti-α-tubulin antibody (α-tub) were used to normalize KCC2 signals and reveal the plasma membrane selectiveness and background of the biotinylation procedure. *B*, Western blot of N2a cells expressing pcDNA3.1 (mock), wild-type KCC2 (WT) and ΔCTD-KCC2 (ΔCTD). Detection with anti-KCC2 chicken ($KCC2_{chk}$) antibody recognizing *N*-terminus of KCC2. *C*, Summary data of surface biotinylation rates (biotinylated/total ratio) for α-tr, KCC2 and α-tub proteins in samples extracted from cells transfected with either WT-KCC2 or ΔNTD-KCC2 and revealed as described in panel *A*. * $p<0.05$, n=5, non-parametric Wilcoxon matched pairs test. *D*, Summary data of surface biotinylation rates for α-tr, KCC2 and α-tub proteins in samples extracted from cells transfected with either WT-KCC2 or ΔCTD-KCC2 and revealed as described in panel *B*. * $p<0.05$, n=6, non-parametric Wilcoxon matched pairs test. Parameters of boxplots are the same as detailed in Figure 1.

FIGURE 8. Scheme of the surface expression of different KCC2 mutants. The deletion of *N*-terminus abolishes plasmalemmal delivery of the transporter, whereas the deletion of *C*-terminus does not interrupt this process. Thus, the *N*-terminus is indispensable for KCC2's surface delivery. The mutant with deleted *C*-terminus is internalized more effectively than the wild-type KCC2 (left panel). We postulate that wild-type KCC2 is stabilized in the plasma membrane using putative anchoring protein that interacts with the *C*-terminus of the transporter (right panel).

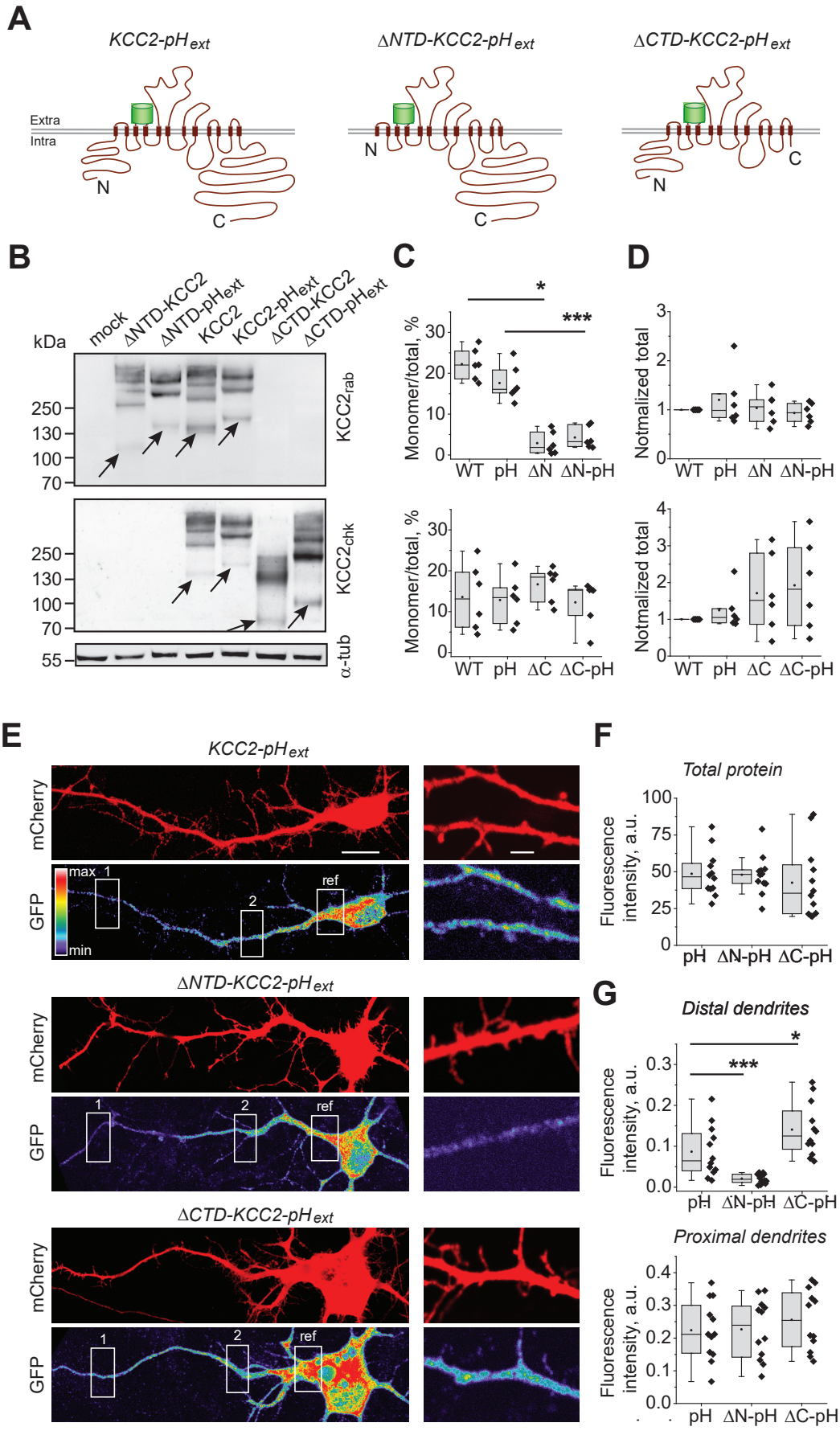

Figure 1

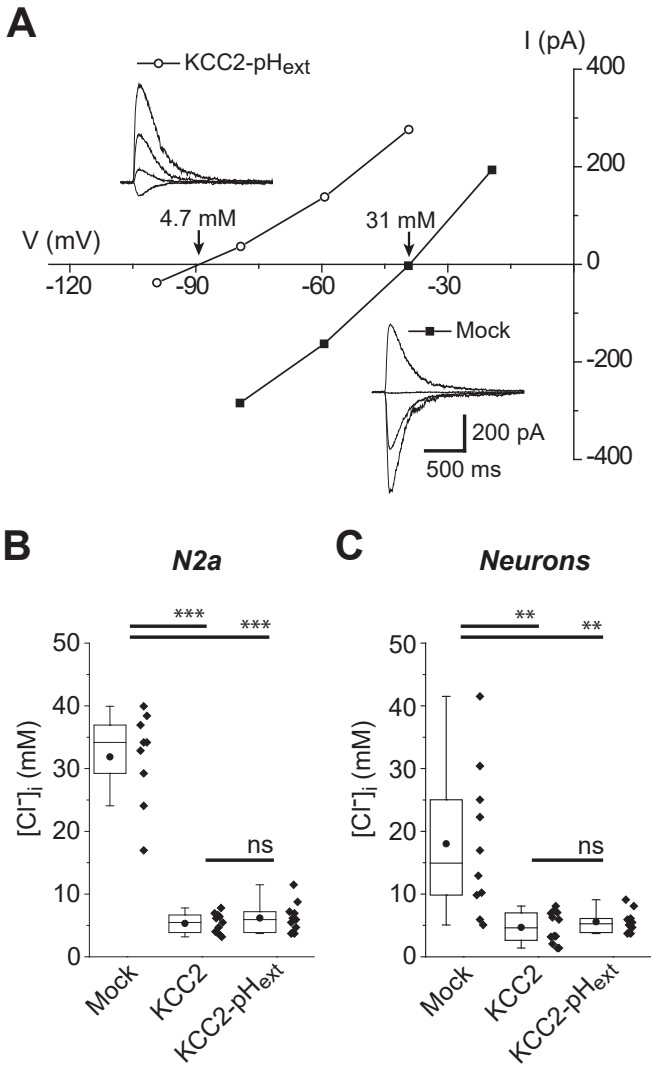

Figure 2

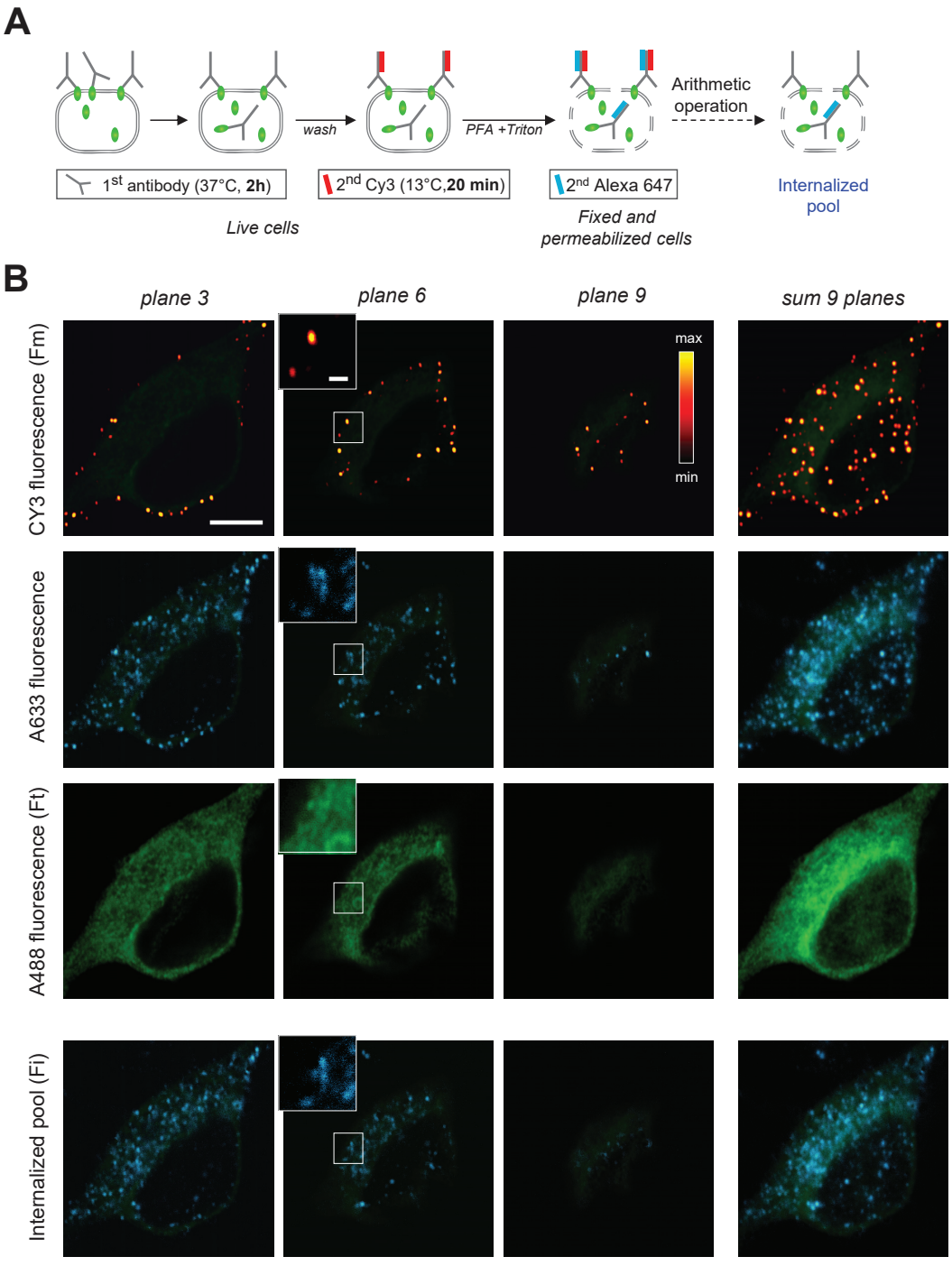

Figure 3

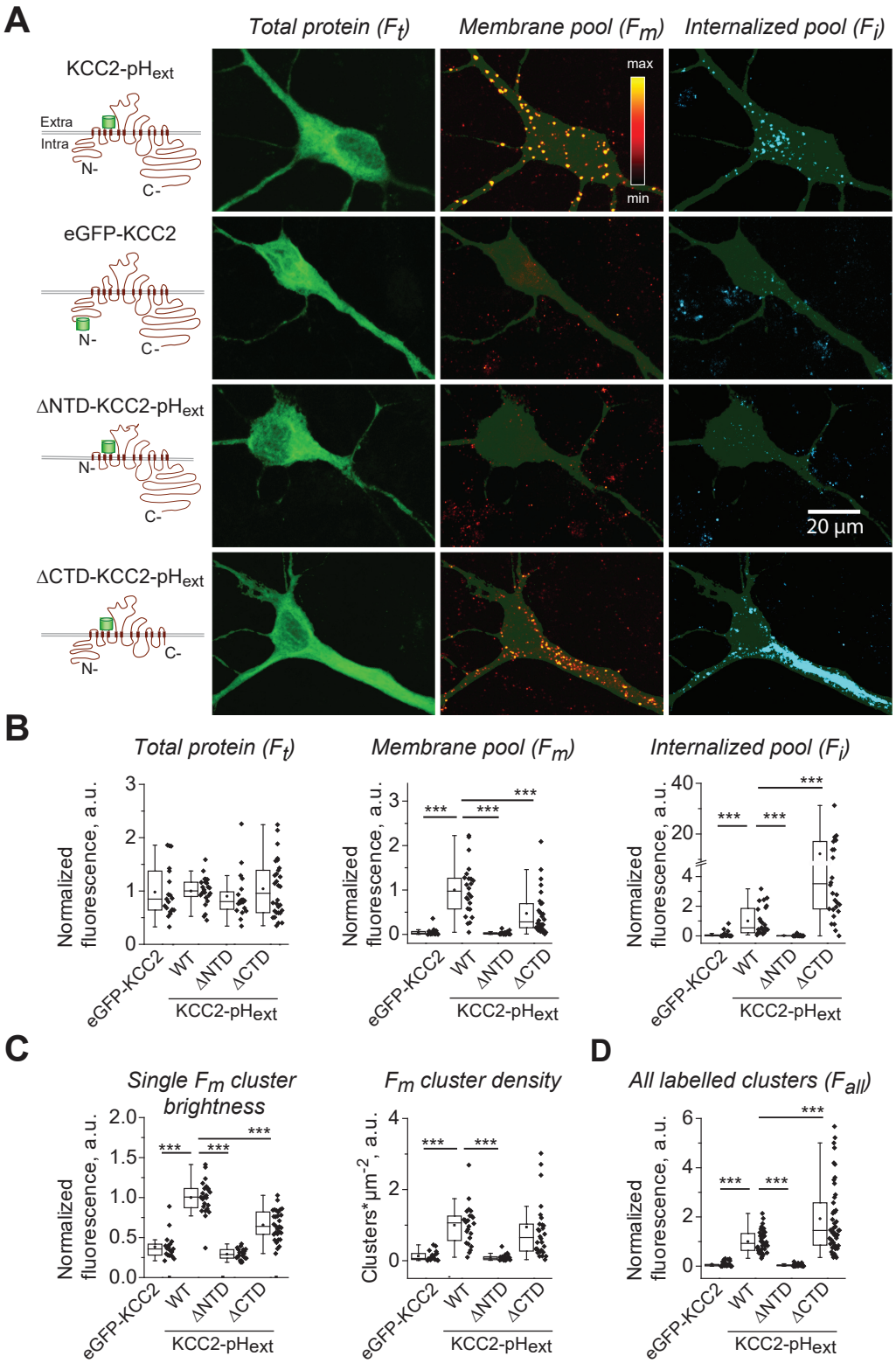

Figure 4

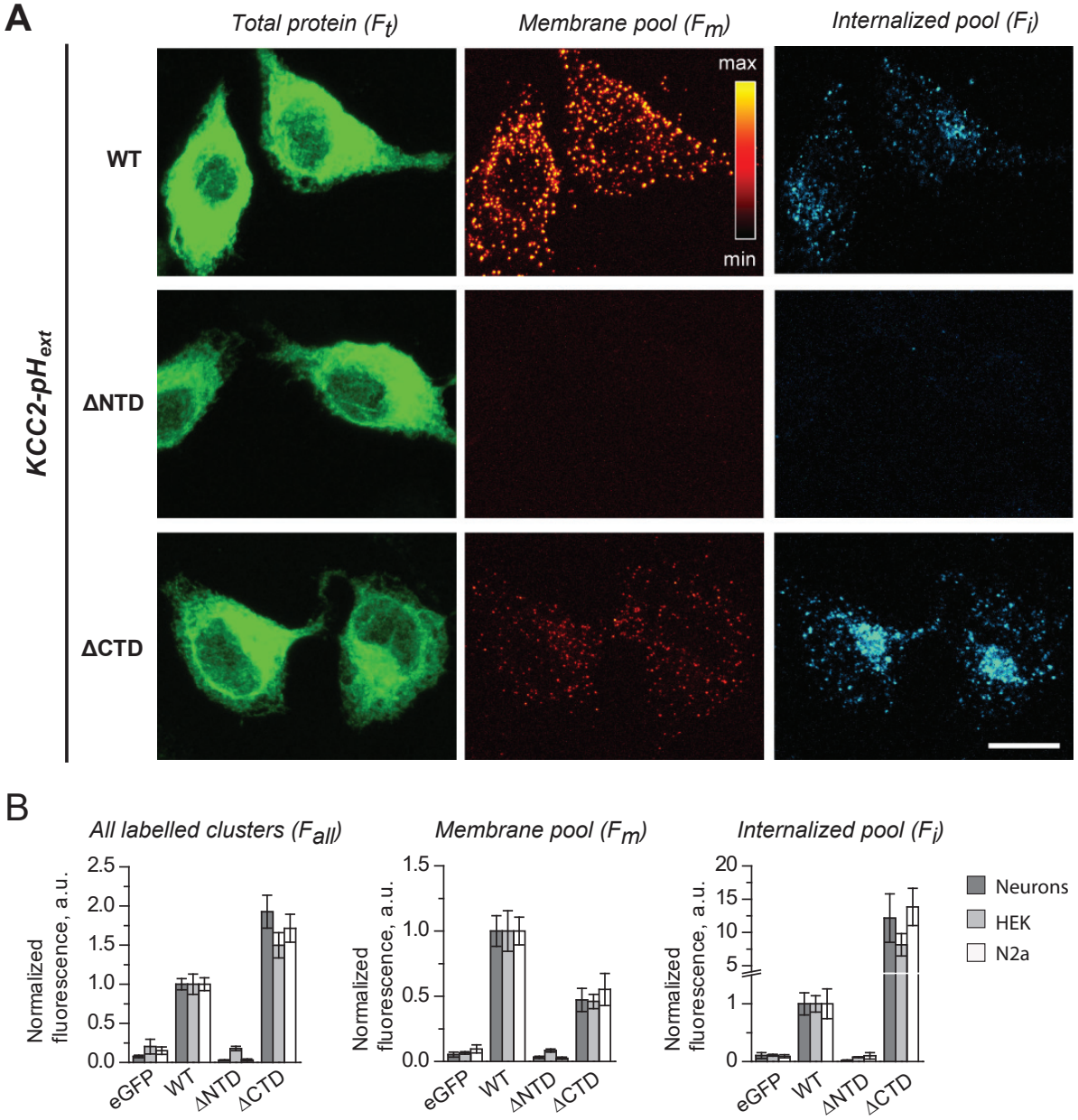

Figure 5

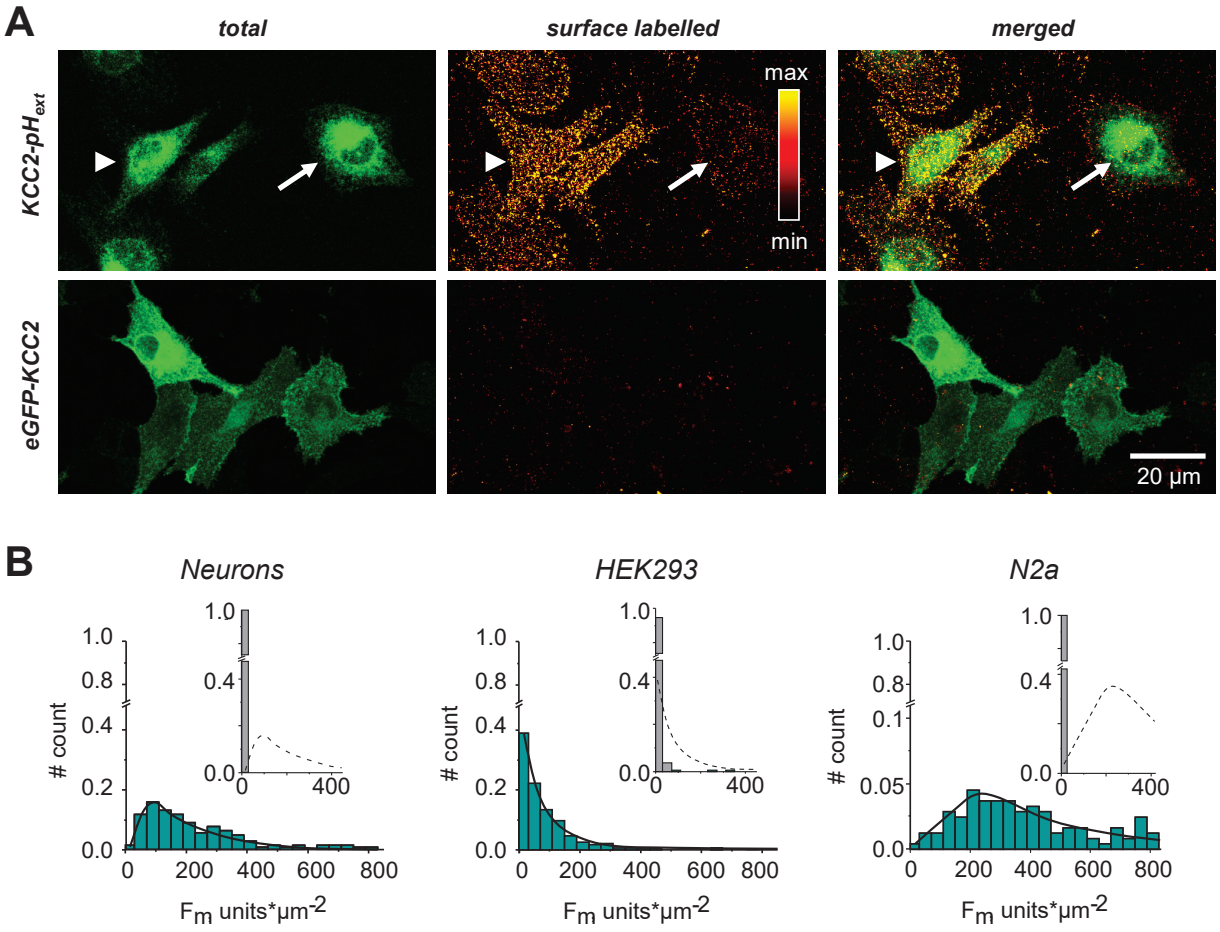

Figure 6

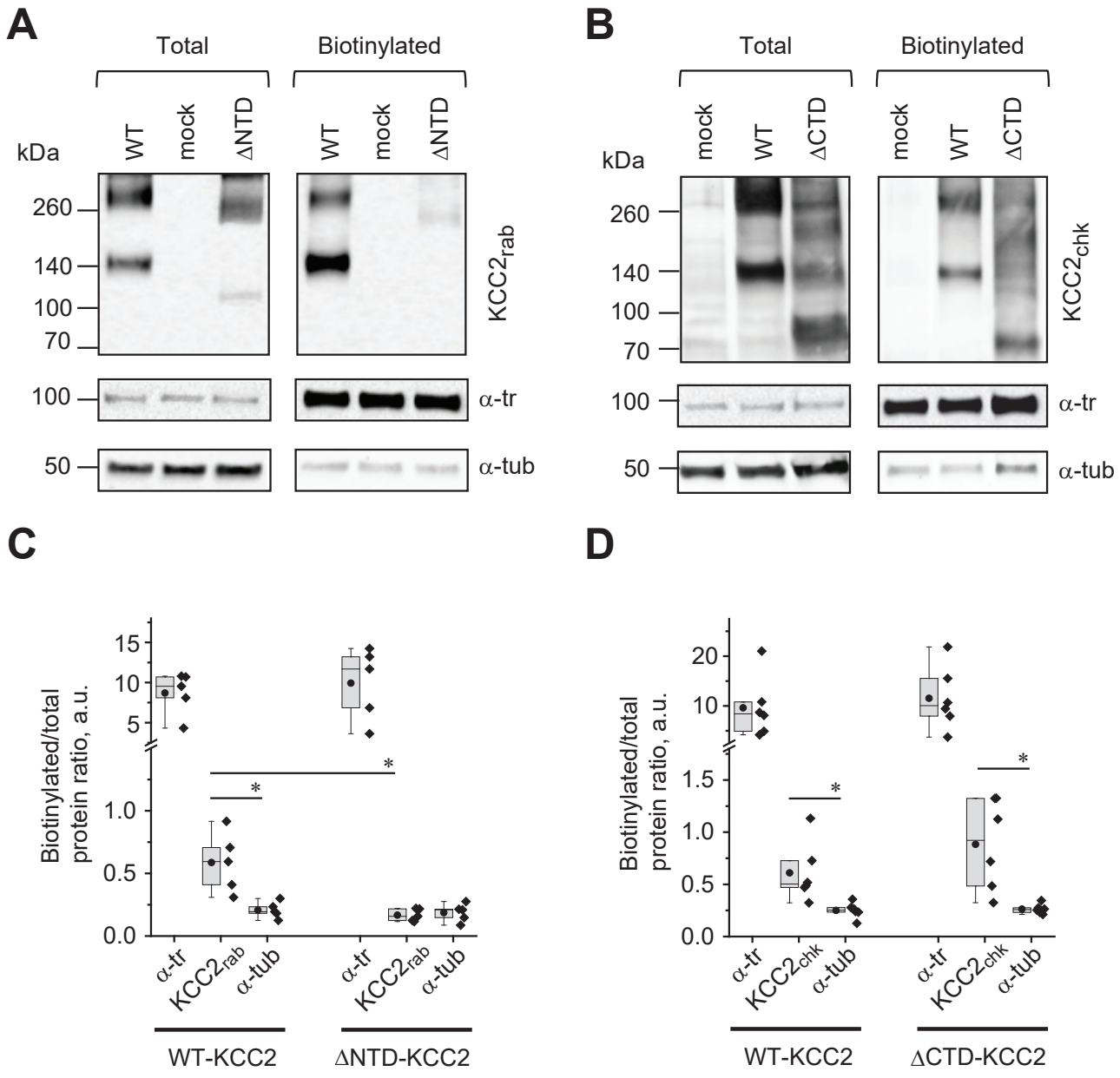

Figure 7

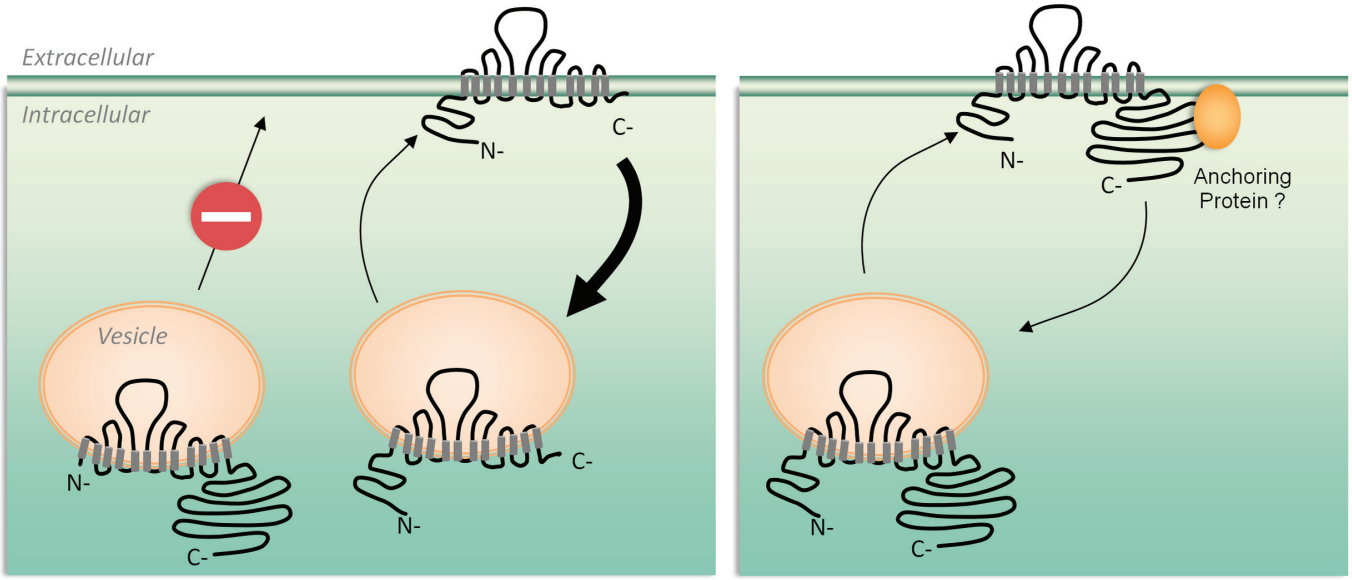

Figure 8

Table 1. Statistical differences among the samples illustrated in Figures 1 and 2.

	Data reference	Data structure	Type of test	Power
a	Fig.1 C, upper panel	Non-normal distribution	Wilcoxon matched pairs test	
	WT vs pH			Z=1.68, n=6; p=0.090
	WT vs ΔN			Z=2.09, n=6; p=0.031
	pH vs ΔN-pH			Z=2.09, n=6; p=0.031
	ΔN vs ΔN-pH			Z=-0.84, n=6; p=0.840
b	Fig.1 C, lower panel	Non-normal distribution	Wilcoxon matched pairs test	
	WT vs pH			Z=0, n=6; p=1.000
	WT vs ΔC			Z=-1.04, n=6; p=0.312
	pH vs ΔC-pH			Z=0, n=6; p=1.000
	ΔC vs ΔC-pH			Z=1.46, n=6; p=0.160
c	Fig.1 D, upper panel	Non-normal distribution	Wilcoxon matched pairs test	
	WT vs pH			Z=-0.21, n=6; p=0.840
	WT vs ΔN			Z=0, n=6; p=1.000
	pH vs ΔN-pH			Z=1.25, n=6; p=0.109
	ΔN vs ΔN-pH			Z=1.35, n=6; p=0.093
d	Fig.1 D, lower panel	Non-normal distribution	Wilcoxon matched pairs test	
	WT vs pH			Z=-0.63, n=6; p=0.563
	WT vs ΔC			Z=-1.26, n=6; p=0.219
	pH vs ΔC-pH			Z=-1.26, n=6; p=0.922
	ΔC vs ΔC-pH			Z=-1.05, n=6; p=0.891
e	Fig.1 F	Non-normal distribution	Mann-Whitney U-test	
	WT vs ΔNTD			U=68, n=12,12; p=0.843
	WT vs ΔCTD			U=93, n=12,12; p=0.242
f	Fig.1 G, upper panel	Non-normal distribution	Mann-Whitney U-test	
	WT vs ΔNTD			U=12, n=12,12; p=5.8e-4
	WT vs ΔCTD			U=36, n=12,12; p=0.040
g	Fig.1 G, lower panel	Non-normal distribution	Mann-Whitney U-test	
	WT vs ΔNTD			U=72, n=12,12; p=0.976
	WT vs ΔCTD			U=62, n=12,12; p=0.562
h	Fig.2 B	Normal distribution	One-way Anova	F(2,28)=118.15, p=2.24e-14
	Mock vs WT		post-hoc Tukey	p=1.70e-13
	Mock vs KCC2-pH_{ext}		post-hoc Tukey	p=3.75e-13
	WT vs KCC2-pH_{ext}		post-hoc Tukey	p=0.89
i	Fig.2 C	Normal distribution	One-way Anova	F(2,29)=12.46, p=1.24e-04
	Mock vs WT		post-hoc Tukey	p=2.36e-04
	Mock vs KCC2-pH_{ext}		post-hoc Tukey	p=8.85e-04
	WT vs KCC2-pH_{ext}		post-hoc Tukey	p=0.95

Table 2. Statistical differences among the samples illustrated in Figure 4.

		Data structure	Type of test	Power
a	Fig.4 B, plot F_t	Non-normal distribution	Mann-Whitney U-test	
	eGFP-KCC2 vs WT			*U*=185, n=19,24; *p*=0.30
	WT vs ΔNTD			*U*=161, n=24,20; *p*=0.06
	WT vs ΔCTD			*U*=357, n=24,30; *p*=0.97
	ΔNTD vs ΔCTD			*U*=274, n=20,30; *p*=0.72
b	Fig.4 B, plot F_m	Non-normal distribution	Mann-Whitney U-test	
	eGFP-KCC2 vs WT			*U*=9, n=19,24; *p*=2.42e-10
	WT vs ΔNTD			*U*=476, n=24,20; *p*=1.36e-11
	WT vs ΔCTD			*U*=568, n=24,30; *p*=1.89e-04
	ΔNTD vs ΔCTD			*U*=26, n=20,30; *p*=4.96e-10
	eGFP-KCC2 vs ΔNTD			*U*=220, n=19,20; *p*=0.4
	eGFP-KCC2 vs ΔCTD			*U*=47, n=19,30; *p*=1.09e-06
c	Fig.4 B, plot F_i	Non-normal distribution	Mann-Whitney U-test	
	eGFP-KCC2 vs WT			*U*=420, n=19,24; *p*=2.28e-07
	WT vs ΔNTD			*U*=476, n=24,20; *p*=1.36e-11
	WT vs ΔCTD			*U*=106, n=24,30; *p*=2.86e-06
	ΔNTD vs ΔCTD			*U*=8, n=20,30; *p*=2.84e-12
	eGFP-KCC2 vs ΔNTD			*U*=230, n=19,20; *p*=0.24
	eGFP-KCC2 vs ΔCTD			*U*=14, n=19,30; *p*=2.58e-08
d	Fig.4 C, single F_m	Non-normal distribution	Mann-Whitney U-test	
	eGFP-KCC2 vs WT			*U*=14, n=19,24; *p*=1.27e-09
	WT vs ΔNTD			*U*=447, n=24,20; *p*=7.95e-12
	WT vs ΔCTD			*U*=647, n=24,30; *p*=5.59e-08
	ΔNTD vs ΔCTD			*U*=14, n=20,30; *p*=2.16e-11
	eGFP-KCC2 vs ΔNTD			*U*=242, n=19,20; *p*=0.15
	eGFP-KCC2 vs ΔCTD			*U*=70, n=19,30; *p*=1.08e-05
e	Fig.4 C, F_m density	Non-normal distribution	Mann-Whitney U-test	
	eGFP-KCC2 vs WT			*U*=16, n=19,24; *p*=2.28e-09
	WT vs ΔNTD			*U*=470, n=24,20; *p*=1.58e-10
	WT vs ΔCTD			*U*=452, n=24,30; *p*=0.11
	ΔNTD vs ΔCTD			*U*=33, n=20,30; *p*=2.25e-09
	eGFP-KCC2 vs ΔNTD			*U*=206, n=19,20; *p*=0.66
	eGFP-KCC2 vs ΔCTD			*U*=58, n=19,30; *p*=3.36e-06
f	Fig.4 D	Non-normal distribution	Mann-Whitney U-test	
	eGFP-KCC2 vs WT			*U*=0, n=33,40; *p*=2.64e-13
	WT vs ΔNTD			*U*=1480, n=40,37; *p*=4.69e-14
	WT vs ΔCTD			*U*=538, n=40,46; *p*=9.56e-04
	ΔNTD vs ΔCTD			*U*=0, n=37,46; *p*=6.56e-15
	eGFP-KCC2 vs ΔNTD			*U*=719, n=33,37; *p*=0.2
	eGFP-KCC2 vs ΔCTD			*U*=0, n=33,46; *p*=4.65e-14

Table 3. Statistical differences among the samples illustrated in Figure 5.

		Data structure	Type of test	Power
a	Fig.5 B, F_{all} HEK	Non-normal distribution	Mann-Whitney U-test	
	eGFP-KCC2 vs WT			*U*=995, n=70,109; *p*=2.18e-19
	WT vs ΔNTD			*U*=11412, n=109,117; *p*=2.48e-29
	WT vs ΔCTD			*U*=4182, n=109,106; *p*=4.32e-04
	ΔNTD vs ΔCTD			*U*=1015, n=117,106; *p*=2.36e-33
b	Fig.5 B, F_{all} N2a	Non-normal distribution	Mann-Whitney U-test	
	eGFP-KCC2 vs WT			*U*=16, n=23,24; *p*=1.13e-10
	WT vs ΔNTD			*U*=552, n=24,23; *p*=1.24e-13
	WT vs ΔCTD			*U*=173, n=24,27; *p*=0.004
	ΔNTD vs ΔCTD			*U*=9, n=23,27; *p*=1.80e-12
c	Fig.5 B, F_m HEK	Non-normal distribution	Mann-Whitney U-test	
	eGFP-KCC2 vs WT			*U*=1076, n=61,109; *p*=8.23e-15
	WT vs ΔNTD			*U*=10352, n=109,117; *p*=1.88e-17
	WT vs ΔCTD			*U*=6428, n=109,106; *p*=0.15
	ΔNTD vs ΔCTD			*U*=2320, n=117,106; *p*=2.34e-17
d	Fig.5 B, F_m N2a	Non-normal distribution	Mann-Whitney U-test	
	eGFP-KCC2 vs WT			*U*=11, n=23,24; *p*=2.42e-11
	WT vs ΔNTD			*U*=546, n=24,23; *p*=3.72e-12
	WT vs ΔCTD			*U*=679, n=24,38; *p*=0.0010
	ΔNTD vs ΔCTD			*U*=33, n=23,38; *p*=2.86e-12
e	Fig.5 B, F_i HEK	Non-normal distribution	Mann-Whitney U-test	
	eGFP-KCC2 vs WT			*U*=1356, n=61,109; *p*=2.40e-11
	WT vs ΔNTD			*U*=10638, n=109,117; *p*=3.26e-14
	WT vs ΔCTD			*U*=2362, n=109,106; *p*=5.77e-15
	ΔNTD vs ΔCTD			*U*=479, n=117,106; *p*=1.19e-32
f	Fig.5 B, F_i N2a	Non-normal distribution	Mann-Whitney U-test	
	eGFP-KCC2 vs WT			*U*=41, n=23,24; *p*=3.03e-08
	WT vs ΔNTD			*U*=548, n=24,23; *p*=1.49e-12
	WT vs ΔCTD			*U*=142, n=24,38; *p*=1.62e-06
	ΔNTD vs ΔCTD			*U*=11, n=23,38; *p*=1.04e-14

Table 4. Statistical differences among the samples illustrated in Figure 7.

		Data structure	Type of test	Power
a	Fig.7 C	Non-normal distribution	Wilcoxon matched pairs test	
	WT, KCC2rab vs WT, Tub			Z=1.89, n=5; p=0.031
	WT, KCC2rab vs ΔNTD, KCC2rab			Z=1.89, n=5; p=0.031
	ΔNTD, KCC2rab vs ΔNTD, Tub			Z=-0.27, n=5; p=0.69
b	Fig.7 D	Non-normal distribution	Wilcoxon matched pairs test	
	WT, KCC2chk vs WT, Tub			Z=2.10, n=6; p=0.016
	WT, KCC2chk vs ΔCTD, KCC2chk			Z=-1.26, n=6; p=0.92
	ΔCTD, KCC2chk vs ΔCTD, Tub			Z=-2.10, n=6; p=0.016